Remote Sensing methodology to assess water quality over Portuguese reservoirs

Vítor Hugo da Silva Neves

Mestrado em Ecologia e Ambiente

Departamento de Biologia

2020

Orientador

Sara Cristina Antunes, Investigadora Auxiliar do Centro Interdisciplinar de Investigação Marinha e Ambiental e Profª Auxiliar Convidada do Departamento de Biologia da Faculdade de Ciências da Universidade do Porto

Coorientador

Giorgio Pace, Investigador do Centro de Biologia Molecular e Ambiental, Universidade do Minho

Assinado por: João José Pradinho Honrado
Identificação: BI10280546
Data: 2020-11-25 às 15:54:12

Todas as correções determinadas pelo júri, e só essas, foram efetuadas.
O Presidente do Júri,

Porto, _____/_____/_____

Dissertação submetida à Faculdade de Ciências da Universidade do Porto, para a obtenção do grau de Mestre em Ecologia e Ambiente, da responsabilidade do Departamento de Biologia, desenvolvida no âmbito do **projeto POCI-01-0145-FEDER-029368**, co-financiado pelo COMPETE 2020, Portugal 2020 e a União Europeia através do ERDF, e pela FCT através de fundos nacionais.

"ReDEFine: a multi-scale and multi-tiered toolbox for assessing ecosystem quality of freshwater REservoirs: briDging the gaps of the watEr Framework dIrEctive approach"

A presente tese foi desenvolvida sob a orientação científica da Doutora Sara Cristina Ferreira Marques Antunes, Professora Auxiliar Convidada do Departamento de Biologia da FCUP e Investigadora Auxiliar do CIIMAR (Centro Interdisciplinar de Investigação Marinha e Ambiental); e coorientação científica do Doutor Giorgio Pace, Investigador do CBMA (Centro de Biologia Molecular e Ambiental), na Universidade do Minho.

COMPETE 2020
FCT Fundação para a Ciência e a Tecnologia
Cofinanciado por: PORTUGAL 2020
UNIÃO EUROPEIA Fundo Europeu de Desenvolvimento Regional
REPÚBLICA PORTUGUESA

Agradecimentos

Primeiramente, gostaria de agradecer à minha orientadora, a Dra. Sara Antunes. Voltou a acolher de braços abertos alguém que já conhecia do estágio, dando-lhe uma oportunidade fantástica na forma de um projeto interessante. Sem a sua paciência, boa vontade, confiança e disponibilidade para ajudar, nada neste trabalho e no meu percurso académico teria sido o mesmo. Gostaria também de agradecer ao meu coorientador, o Dr. Giorgio Pace. Desde o primeiro dia mostrou um entusiasmo contagiante relativamente ao projeto; sem a sua prontidão para ajudar a resolver as minhas dúvidas tudo teria sido imensamente mais difícil, senão impossível. Obrigado por procurar sempre oferecer novas perspetivas em torno do objetivo e por "descomplicar" o que parece complicado. Com esta equipa senti-me em casa, senti que aprendi imenso e ressurgiu uma curiosidade científica que previamente julgava estar a perder. Foi fantástico trabalhar convosco. Agradeço ainda ao Prof. Nuno Formigo; sem os seus conselhos quando mais precisei certamente não teria realizado este trabalho.

À restante equipa do Fresh lab; apesar das circunstâncias em que vivemos não terem permitido/promovido as melhores condições para convivermos, em todos os momentos que estive convosco foram uma boa companhia, sempre prestáveis e prontos a animar os meus dias de trabalho. Obrigado por tudo isto e que o vosso futuro e o do laboratório seja próspero.

Aos colegas do “Laboratorio de Procesado de Imágenes” (LPI) da Universidade de Valência, obrigado pela disponibilidade e pela partilha de conhecimentos. Sem a vossa ajuda este trabalho não teria tido este rumo.

Aos amigos que me acompanharam mais de perto ao longo do mestrado - Diana, Marcus, Bárbara e Francisco; sem vocês esta aventura teria sido mais difícil, menos memorável e certamente mais aborrecida. Desde a diversão das nossas cartadas no bar aos imensos stresses na realização de trabalhos de grupo, todos os momentos foram importantes para mim e fizeram-me crescer. Apesar das nossas diferenças fomos capazes de sair inteiros e juntos no final de contas. Espero que o futuro não nos separe demasiado e também que vos reserve imensas felicidades. De vós levo boas memórias.

À minha “piquena” afilhada; o tempo passa a voar e é impiedoso! Mesmo afundados em trabalho, mais que nunca, arranjamos sempre tempo para ficarmos a par das novidades na vida de cada um. Muito obrigado por ouvires os meus problemas e também por partilhares os teus comigo. Obrigado pela confiança e pela grande amizade. Nunca me falhaste e tenho para ti reservado um lugar especial no meu coração, sempre. Muito obrigado Bita!

Aos meus Assíduos; sei que devido às diferentes vidas que cada um de nós leva, naturalmente estamos pouco tempo juntos. Contudo, esses poucos momentos trazem sempre um sentimento de felicidade e saudade. Espero que nunca nos separemos de verdade, pois creio que será uma grande perda para todos. Obrigado e que no futuro consigamos ser mais “Assíduos”.

Às hienas mais próximas que me acolheram de volta numa altura importante. Obrigado por voltarem a animar os meus dias, obrigado pelas piadas, memes, desabafos e compreensão. Conto convosco para criar muitas mais memórias.

Ao Rodrigo, que é sempre o primeiro a perguntar como tenho andado e que novidades tenho. Sei que sempre que precisar terei um ombro amigo em ti! Muita sorte na tua nova aventura e muito obrigado por estes anos de amizade.

A um dos pilares mais importantes na minha vida. Diana, foste a melhor surpresa que este mestrado me podia trazer. Já me aturas diariamente há muito tempo; todos os dias me animas, me ouves, me compreendes e me ajudas. Obrigado por fazeres de mim uma pessoa melhor e obrigado por me cativares. Obrigado por ultrapassarmos sempre os maus momentos juntos e obrigado por teres orgulho em mim. Podia ficar aqui todo o dia a agradecer-te por mil e uma coisas, mas sei que entendes o que significa o meu “Muito obrigado!”.

E finalmente, à minha família. Muitas vezes são os primeiros a me "consumir o juízo", mas são também os que mais se preocupam comigo e os primeiros a querer contribuir para a minha felicidade. Foi graças a vocês e a todos os vossos esforços que estou na posição que estou hoje e por isso vos estou eternamente grato. Sei que sou muito “chato” e que também eu vos "consumo o juízo", mas quero que saibam que vos adoro incondicionalmente. Aos meus pais, acreditem que estou ciente de todo o trabalho que deu criar dois filhos, sem nunca lhes faltar nada e com a melhor educação possível.

Sempre foram e sempre serão os meus super-heróis, apesar de o nunca ter dito. À minha irmã: és uma grande “chata”, mas sei que sempre que o és estás a tentar que eu melhore. Foste sempre uma segunda mãe e a melhor irmã que alguma vez podia ter pedido. E por fim, obrigado por me teres arranjado um cunhado excelente e que também me ajuda, com todo o gosto, sempre que preciso; muito obrigado ao João por ser sempre “5 estrelas” e por cuidar bem da minha irmã. Apesar do sossego, já tenho saudades de vos ter cá em casa.

A todos aqueles que me ajudaram de qualquer modo, tenham sido mencionados ou não, muito obrigado!

Resumo

As albufeiras estão sujeitas a pressões antropogénicas, tornando-se cada vez mais degradadas. Estas providenciam habitats a muitas espécies bem como serviços de ecossistema fundamentais. Deste modo, é necessário avaliar mudanças em albufeiras e compreender a magnitude e consequências das mesmas. A Diretiva Quadro da Água (DQA) define métricas para avaliar a qualidade da água que requerem trabalho de campo seguido de trabalho laboratorial, sendo um processo lento e monetariamente exigente. Técnicas de deteção remota podem providenciar uma solução complementar que é monetariamente eficiente, prática, de ampla cobertura e passível de realizar com frequência. Neste estudo pretende-se avaliar a utilidade de técnicas de deteção remota para avaliar o potencial ecológico de duas albufeiras portuguesas – Aguieira e Alqueva – estabelecido pela DQA. Amostragens foram realizadas em quatro estações: Outono de 2018, Primavera de 2019, Outono de 2019 e Primavera de 2020. Foram selecionadas e descarregadas imagens de Nível 1-C do Sentinel-2 a partir do EarthExplorer, dizendo respeito às quatro estações e às duas albufeiras. De seguida, as imagens foram processadas com o processador de correções atmosféricas C2RCC, na SNAP, para estimar [Chl *a*] e [TSM]. Todos os dados foram analisados com o software *R*. Foram comparados dados *in situ* e de satélite através de Correlações de Spearman, das métricas "Normalized Root Mean Square Error" (NRMSE) e "Normalized Men Bias Error" (NMBE) e Análises de Componentes Principais (PCA). Os resultados das correlações não foram estatisticamente significativos, excetuando quando foi usado o produto TSM-S60m no Alqueva, que permitiu uma correlação modesta com os dados *in situ*. De modo geral, os erros relativos (NRMSE) e sistemáticos (NMBE) foram mais baixos para a Aguieira do que para o Alqueva. As PCAs permitiram avaliar diferenças sazonais e entre albufeiras. Os resultados demonstraram que as diferenças sazonais foram independentes do uso de dados de satélite e que diferenças espaciais parecem ter maior impacto nos resultados do que diferenças temporais. A deteção remota de águas interiores continua a enfrentar muitos desafios. Contudo, estudos recentes nesta área são um marco de avanços a nível de precisão, aplicação e robustez de produtos de deteção remota em águas interiores. Com este estudo espera-se não só contribuir para estes avanços, como também promover novos conhecimentos relacionados com águas interiores, em particular albufeiras.

Palavras-chave: DQA, Qualidade de água, Albufeira, Deteção remota via satélite, C2RCC, Clorofila *a*, Matéria orgânica total suspensa

Abstract

Reservoirs are subject to anthropogenic stressors, becoming increasingly degraded. They provide habitats to a large amount of species as well as critical ecosystem services. Therefore, it is necessary to evaluate changes within reservoirs and understand their magnitude and implications towards the ecosystem. The Water Framework Directive (WFD) defines several metrics to assess water quality that require field work followed by laboratory analyses, making the process slow and expensive. Remote sensing techniques can provide a complementary solution that is cost effective and practical, has a broad coverage and that can be frequently executed. In this study we intend to validate the utility of remote sensing techniques to assess the ecological potential of two Portuguese reservoirs – Aguieira and Alqueva -, established by the WFD. Samples were carried out in four seasons: Autumn of 2018, Spring of 2019, Autumn of 2019 and Spring of 2020. Sentinel-2 Level 1-C imagery was selected and later downloaded from EarthExplorer concerning the four seasons and the different study sites. Then, images were processed with C2RCC atmospheric correction processor, in SNAP, to estimate [Chl *a*] and [TSM]. All data was analysed in *R* software. *In situ* and satellite data were compared through Spearman's correlations, Normalized Root Mean Square Error (NRMSE) and Normalized Mean Bias Error (NMBE) metrics and Principal Component Analysis (PCA). Spearman's correlations results were not statistically significant, except using TSM-S60m in Alqueva which had a modest correlation with *in situ* data. Relative (NRMSE) and systematic (NMBE) errors were generally lower in Aguieira than in Alqueva. PCAs allowed to assess seasonal changes and changes between reservoirs. Results showed that seasonal changes seem to be independent of the use of satellite estimated data and that spatial differences seem more impactful than temporal differences. Inland water remote sensing has faced, and continues to face, many challenges. However, the current advancements in this field of study have marked improvements in the accuracy, applicability and robustness of remote sensing products for inland waters. By studying the validity of applying C2RCC to these two reservoirs we hope not only to contribute to these improvements, but also bring forth new knowledge concerning inland waters, and particularly reservoirs.

Keywords: WFD, Water quality, Reservoir, Satellite remote sensing, C2RCC, Chlorophyll *a*, Total suspended matter

Table of contents

Table index

Figure index

Abbreviations

Abbreviation	Description
CHABs	Cyanobacterial Harmful Algal Blooms
WFD	Water Framework Directive
EU	European Union
Chl *a*	Chlorophyll *a*
NAP	Nonalgal Particles
CDOM	Coloured Dissolved Organic Matter
PC	Phycocyanin
TSM	Total Suspended Matter
MSI	Multi-Spectral Instrument
AC	Atmospheric Correction
[Chl *a*]	Concentration of Chlorophyll *a*
MERIS	MEdium Resolution Imaging Spectrometer
CLC	CORINE Land Cover
TSS	Total Suspended Solids
USGS	United States Geological Survey
VIS	Visible
NIR	Near-Infrared
C2RCC	Case 2 Regional Coast Colour
TOA	Top-of-Atmosphere
SNAP	Sentinel Application Platform
AOI	Area of Interest
[TSM]	Concentration of Total Suspended Matter
NRMSE	Normalized Root Mean Squared Error
NMBE	Normalized Mean Bias Error
Log	Logarithmic
PCA	Principal Component Analysis
C2R	Case 2 Regional
IOPs	Inherent Optical Properties

1. Introduction

The term “Inland waters” is used to describe interior water bodies such as lakes, reservoirs, rivers, ponds, wetlands and even coastal areas. These environments have a large variety of shapes and sizes, along with physical, chemical and optical properties (Mishra *et al.,* 2017). Despite only covering a relatively small area of the planet’s surface, inland waters are of great importance for the numerous critical functions they play - notably, providing ecosystem services such as food provisioning, nutrient cycling and climate regulation (Pekel *et al.,* 2016).

Historically, inland waters have been a popular place for humans to live nearby, providing them with a water source that serves as a recreation and transportation resource (Corrigan *et al.,* 2009). In addition to providing ecosystem services, as previously mentioned, these water bodies also emerge as a limiting factor in both quantity and quality for human development and ecological stability (Corman, 2017). Furthermore, inland water bodies act as sentinels of the ever-changing environment around them, reporting the status of phenomena such as climate change, developmental pressure, and land use and land cover change (Mishra *et al.,* 2017).

However, inland waters also provide a ‘convenient’ receptacle for waste disposal. Currently, freshwater ecosystems show an increase in degradation due to human activities. Soil occupation and activities such as agriculture, urbanization and industrial affairs comprise actions already described to affect these water bodies (Corrigan *et al.,* 2009). Events like deforestation and reduction of vegetation cover, nutrient pollution, drought and engineered modifications to the watershed act in synergy causing negative impacts in water quality. Indeed, these activities allow the acceleration of eutrophication, proliferation of toxic blue-green algae, extreme turbidity and deterioration of water clarity, among other harmful effects to human and animal health (Mishra *et al.,* 2017; Paerl & Huisman, 2008; Qin *et al.,* 2007).

Consequences of the eutrophication of inland waters include the occurrence of cyanobacterial harmful algal blooms (CHABs) (Merel *et al.,* 2013). Nowadays, CHABs have become a major worldwide issue that is intensifying in both frequency and magnitude (Hudnell *et al.,* 2008; Paerl & Huisman, 2008). They have significant environmental impacts since high cyanobacterial biomass can out-compete other organisms for resources. In addition, the conditions that develop during CHABs die off and decomposition contribute to the degradation of aquatic habitats and compromise ecosystem sustainability (Kirk & Gilbert, 1992; Müller-Navarra *et al.,* 2000; Wilson *et al.,* 2006). Furthermore, many cyanobacteria can produce a variety of toxins and bioactive

compounds, which pose a potential risk to human health (De Figueiredo *et al.,* 2004; Visser *et al.,* 2005).

Reservoirs are a distinct example of an inland water body. They are described by the European Water Framework Directive (WFD) as heavily modified water bodies due to physical alterations caused by human activity, substantially changing them in character (European Community, 2000). Although all reservoirs are built to store water, their functions may differ. Depending on their management, reservoirs can be used for at least five major purposes: irrigation, hydroelectricity production, standard water storage, flood control and/or recreation (Nilsson, 2013).

Much like other inland water bodies, reservoirs are subject to diverse anthropogenic stressors. Therefore, it is necessary to evaluate reservoir ecosystem changes, to understand the magnitude and implications of these alterations and if they are reversible (Scheffer & Carpenter, 2003). In order to protect and manage these aquatic ecosystems, the WFD requires each European Union (EU) member state to assess the ecological potential of their reservoirs (European Community, 2000). Traditionally, the ecological status of water bodies is defined according to their biological, chemical and physical characteristics in comparison to reference values (Blabolil *et al.,* 2016). However, the evaluation of ecological potential in reservoirs is remarkably challenging due to their complex nature, that represents an environment different from lakes and rivers, and due to the lack of an undisturbed reference status (Blabolil *et al.,* 2016; Irz *et al.,* 2002; Wetzel, 2001). Consistent monitoring in water bodies is essential in fulfilling the EU WFD, but traditional *in situ* methods (e.g. water sample collection and laboratory analysis) are often very time and money consuming to estimate the quality of water on a regular basis (Ansper & Alikas, 2019).

Since the 1960s, remote sensing techniques have been used to monitor aquatic environments by analysing ocean colour under the assumption that chlorophyll *a* (Chl *a*) (a proxy for phytoplankton biomass) and surface water temperature could be estimated remotely (Gordon, 1988; Morel & Gordon, 1980). However, the application of remote sensing techniques to inland waters can be significantly different from open ocean waters, mainly because of their different shapes and sizes, the comparably more significant impact of border effect in inland waters and the variable composition of water components. The presence of multiple constituents at different scales [i.e. phytoplankton, nonalgal particles (NAP), coloured dissolved organic matter (CDOM) and detritus] along with the complex interactions among themselves and anthropogenic actions result in less success of remote sensing techniques for monitoring inland water quality compared to open water in oceans (Mishra *et al.,* 2017). Alternatively, satellite

remote sensing techniques have been used as an effective tool for supporting the implementation of the WFD, by deriving phytoplankton and cyanobacterial pigments such as Chl *a*, Phycocyanin (PC), Total Suspended Matter (TSM) and CDOM (Giardino *et al.,* 2014).

Recently, few studies have tried to develop new methodologies for ecological status assessment of aquatic ecosystems, particularly reservoirs (Blabolil *et al.,* 2016). The few assessment systems developed for reservoirs have, so far, not been applied to an area larger than a single country (Han *et al.,* 2014; Jennings *et al.,* 1995; Navarro *et al.,* 2009). However, in Europe there are some examples of studies that used satellite remote sensing techniques to assess inland water bodies (e.g. Potes *et al.,* 2018; Ansper & Alikas, 2019; Sòria-Perpinyà *et al.,* 2019). These studies have different goals and use distinct methodologies, revealing the many capabilities of these techniques.

Ansper and Alikas (2019) used 89 Estonian lakes in a study that aimed to analyse the suitability of Sentinel-2 MultiSpectral Instrument (MSI) data to monitor water quality in inland waters. This work tested various atmospheric correction (AC) processors to remove the influence of atmosphere, as well as comparing and developing a Chl *a* algorithm to estimate the ecological status of water in Estonian lakes. Initial results showed that the Sentinel-2 MSI is suitable for estimating Chl *a* and tracking spatial and temporal dynamics in the lakes. Nonetheless, despite being able to provide complementary information to *in situ* data to support WFD monitoring requirements, it is important to note that ACs are sensitive to surrounding land and often fail in narrow and small lakes.

In the Iberian Peninsula, Sòria-Perpinyà *et al.* (2019) worked on Albufera de València - a hypertrophic lake in Valencia, Spain - that aimed to demonstrate the validity of an algorithm for Chl *a* concentration ([Chl *a*]) retrieval from Sentinel-2's (A and B) MSI. This work was carried out using images from 2016 and 2017, and an AC was performed followed by the estimate of [Chl *a*] using an algorithm developed by Soria *et al.* (2017). Estimated data was validated against field samples, achieving very good results. With these results, the authors were able to infer that the temporal evolution of [Chl *a*] variations follows an annual bimodal pattern.

In Portugal, Potes *et al.* (2018) used the Alqueva reservoir as a study site to assess the use of the Sentinel-2 MSI for water quality monitoring. The team ahead of this work had already been working with Alqueva water quality monitoring since 2006, using MEdium Resolution Imaging Spectrometer (MERIS) multispectral radiometer on-board of ENVISAT-1. In this study, previous algorithms developed by the team for MERIS were tested for the Sentinel-2 MSI for water turbidity, [Chl *a*] and cyanobacteria

density. The results were compared to *in situ* sampling data and laboratory analysis data. In the end, despite the set of algorithms being applied with good results, some tuning was still required to make use of the full potential of the MSI. Nevertheless, this study is a good example of the possible portability between algorithms developed for different instruments.

According to several studies remote sensing techniques could be crucial in the ecological status/potential assessment of inland waters. As opposed to using exclusively traditional field-based methods to monitor water quality, remote sensing offers a comparatively low-cost, high frequency, spatially extensive and practical complement for water quality assessment and monitoring (Duan *et al.,* 2010; Hadjimitsis & Clayton, 2009). As a result, the development of new remote sensing techniques or fine-tuning of existing ones is essential to accurately monitor inland water resources and isolate the natural and anthropogenic stressors (Mishra *et al.,* 2017).

In a perspective of compliance with the WFD and for the more practical and regular water quality assessment of reservoirs, this study aims to apply and validate a remote sensing approach for evaluating water quality in two Portuguese reservoirs. As well, this study will focus on answering questions related to seasonal changes and the portability of the methodology.

2. Material and methods

2.1 Study sites

Two Portuguese reservoirs were selected to conduct this study within the ongoing project ReDEFine - a recent project that makes use of multi-scale and multi-step tools for the assessment of reservoir water quality, to fill existing gaps in the current approach by the WFD (POCI-01-0145-FEDER-029368). The group of reservoirs selected was: Aguieira - reservoir included in the inter-calibration study for the WFD - and Alqueva - one of the largest freshwater reservoirs in the Iberian Peninsula (Fig. 1). For the *in situ* data retrieval, several sampling points were selected at each location (4 in Aguieira reservoir - Fig. 2, and 5 in Alqueva reservoir - Fig. 3).

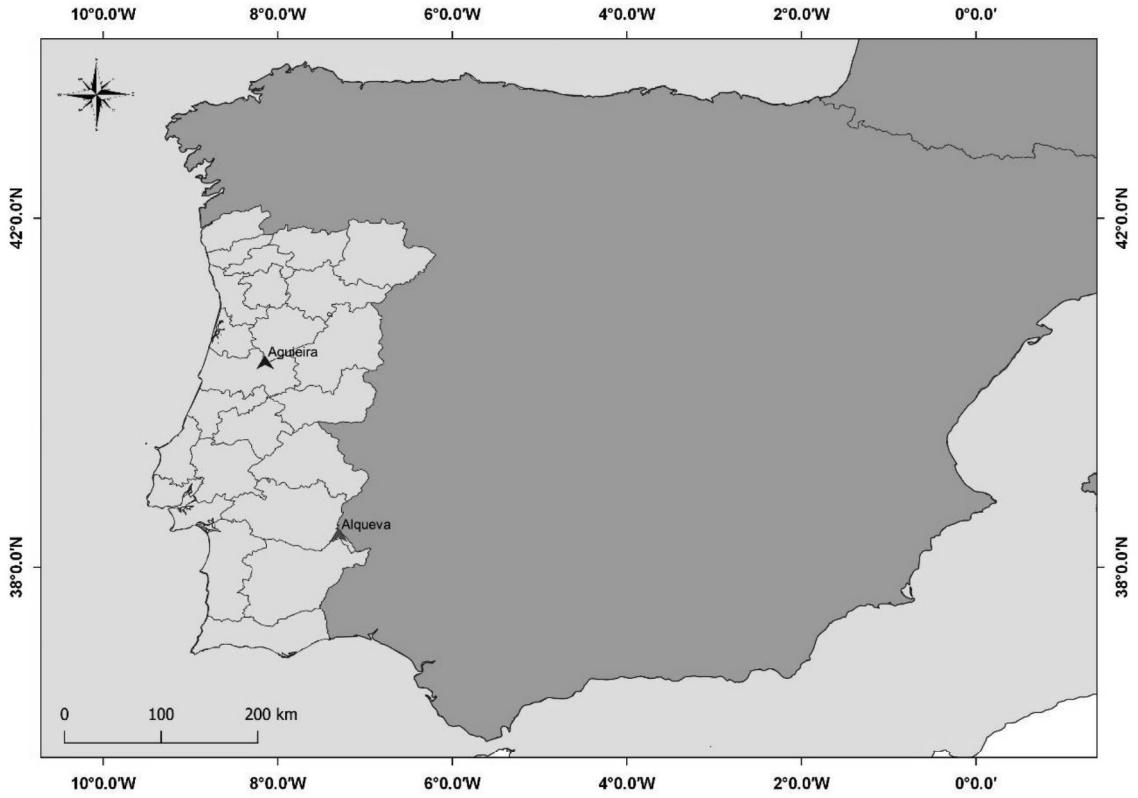

Fig. 1 - Iberian Peninsula. Markers represent the reservoirs used as study sites in this study.

Aguieira reservoir is in Coimbra district - central Portugal - and belongs to the Mondego hydrographic basin (Fig. 2). Its construction was finished in 1981 and it has multiple purposes: production of hydroelectricity, storage, flood control, water supply and irrigation. The reservoir has an area of 20000 x 1000 m^2 and gross capacity of 423000 x 1000 m^3 (https://cnpgb.apambiente.pt/gr_barragens/gbportugal/FICHAS/Aguieiraficha.htm). According to Copernicus' CORINE Land Cover (CLC) 2018, the

areas around Aguieira's sampling points are mainly occupied by broad-leaved forest, land principally occupied by agriculture, significant areas of vegetation, mixed forest and transitional woodland-shrub (https://land.copernicus.eu/pan-european/corine-land-cover/clc2018).

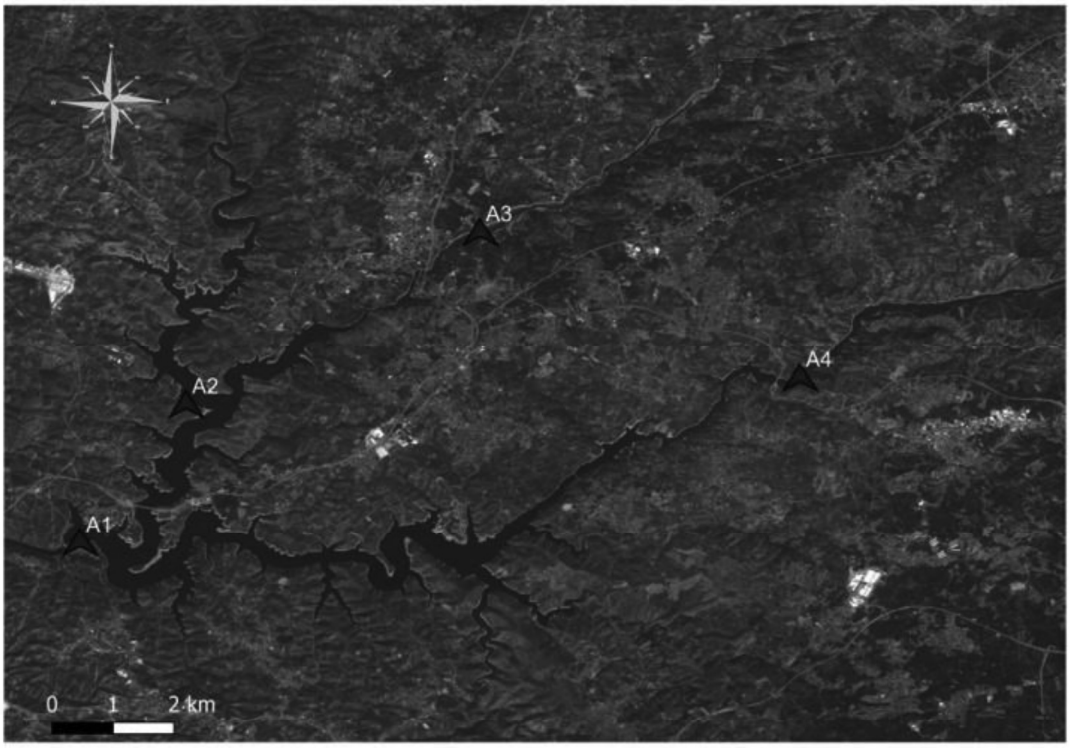

Fig. 2 - Aguieira reservoir, Mondego hydrographic basin, at Coimbra. Sampling Points: A1 (40º20'27.942" N, 8º11'38.616" W), A2 (40º22'01.884" N, 8º10'28.283" W), A3 (40º24'03.488" N, 8º07'01.150" W) and A4 (40º22'22.256" N, 8º03'19.055" W).

Alqueva reservoir is in Beja district - southern Portugal - and belongs to the Guadiana hydrographic basin (Fig. 3). Its construction was finished in 2002 and it has multiple purposes: production of hydroelectricity, storage, water supply and irrigation. The reservoir has an area of 250000 x 1000 m^2 and gross capacity of 4150000 x 1000 m^3 (https://cnpgb.apambiente.pt/gr_barragens/gbportugal/FICHAS/Alquevaficha.htm). According to Copernicus' CLC 2018, the areas around Alqueva's sampling points are mainly occupied by industrial or commercial units, non-irrigated arable lands, permanently irrigated land, fruit trees and berry plantations, olive groves,

complex cultivation patterns, agro-forestry areas, broad-leaved forest and coniferous forest (https://land.copernicus.eu/pan-european/corine-land-cover/clc2018).

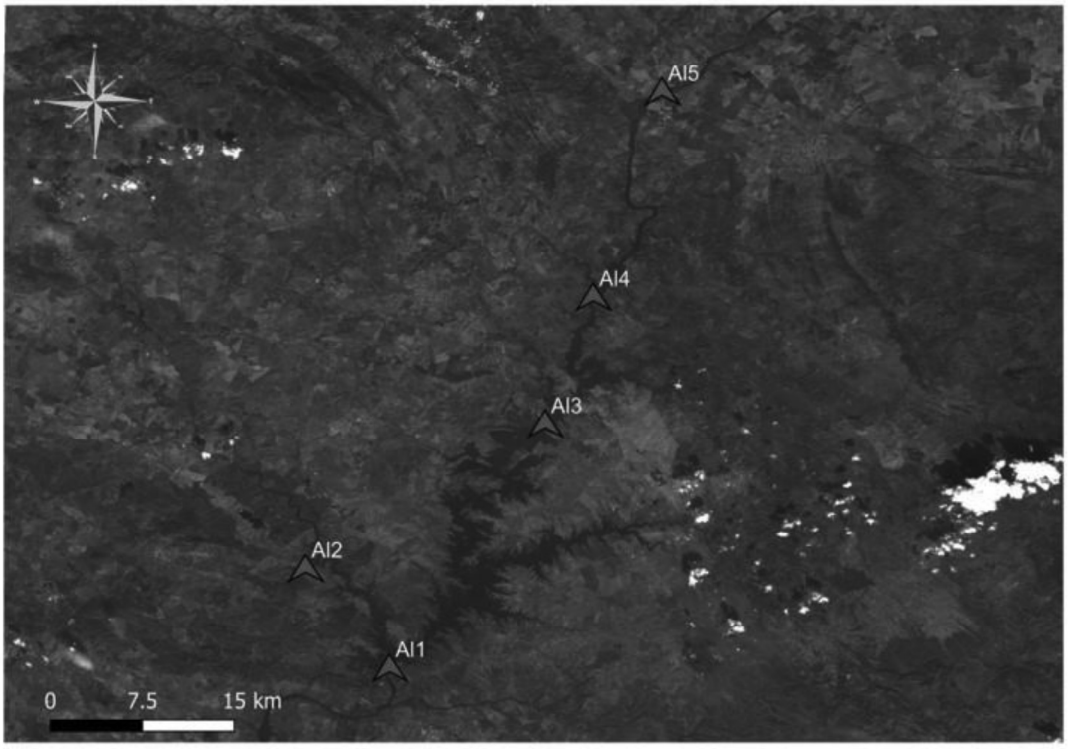

Fig. 3 - Alqueva reservoir, Guadiana hydrographic basin, at Beja. Sampling Points: Al1 (38º12'07.957" N, 7º29'19.717" W), Al2 (38º17'35.785" N, 7º33'41.484" W), Al3 (38º25'58.085" N, 7º21'03.721" W), Al4 (38º32'49.092"' N, 7º18'13.988"' W) and Al5 (38º44'15.763" N, 7º14'15.144" W).

2.2 *In situ* data retrieval

All *in situ* variables used in this study are presented in Table 1. The samplings were carried out in four periods across 2018, 2019 and 2020 (Table 2). *In situ*, with a multiparameter probe (Multi 3630 IDS SET F), some general physical and chemical parameters were measured sub superficially: pH, oxygen concentration (O_2) ($mg.L^{-1}$ and %), conductivity (Cond) ($\mu S.cm^{-1}$) and temperature (Temp) (°C).

At each site, water samples were collected and transported to the laboratory under thermal conditions (at 4 °C and in the dark) for further analysis. For determination of the content of Total Suspended Solids (TSS) and Chl *a*, water was filtered through a Whatman GF/C filter (47 mm diameter and 1.2 µm pore). Three filters with the seston of each sample were used to determine the TSS according to APHA (1989). Chl *a* extraction was performed according to Lorenzen (1967) method.

Table 1 - All *in situ* variables, their acronyms and units.

Variable	Acronym	Units
pH		
Oxygen concentration	O_2	$mg.L^{-1}$ and %
Conductivity	Cond	$\mu S.cm^{-1}$
Temperature	Temp	ºC
Total Suspended Solids	TSS	$mg.L^{-1}$
Chlorophyll *a*	Chl *a*	$\mu g.L^{-1}$
Biochemical Oxygen Demand	BOD_5	$mg.L^{-1}$
Volatile Suspended Solids	VSS	$mg.L^{-1}$
Turbidity	Turb	m
Dissolved Organic Carbon	DOC	m^{-1}
Title Hydrometric	TH	ºf
Iron	Fe	$\mu g.L^{-1}$
Manganese	Mn	$\mu g.L^{-1}$
Arsenic	As	$\mu g.L^{-1}$
Cadmium	Cd	$\mu g.L^{-1}$
Copper	Cu	$\mu g.L^{-1}$
Mercury	Hg	$\mu g.L^{-1}$
Nickel	Ni	$\mu g.L^{-1}$
Lead	Pb	$\mu g.L^{-1}$
Zinc	Zn	$\mu g.L^{-1}$
Chemical Oxygen Demand	COD	$mg.L^{-1}$
Ammonium	NH_4	$mg.L^{-1}$
Kjedahl Nitrogen	N	$mg.L^{-1}$
Nitrate	NO_3	$mg.L^{-1}$
Nitrite	NO_2	$mg.L^{-1}$
Phosphorus	P	$mg.L^{-1}$

2.3 Satellite imagery data retrieval

The satellite images used in this study were captured by Sentinel-2 A and Sentinel-2 B, the two polar-orbiting satellites that comprise the Copernicus Sentinel-2 mission. This mission aims at monitoring variability in land surface conditions and makes use of its wide swath width (290 km) and high revisit time (5 days with the two satellites under cloud-free conditions at the equator, which results in 2-3 days at mid-latitudes) to support monitoring of Earth's surface changes (https://sentinel.esa.int/web/sentinel/missions/sentinel-2). Each satellite is equipped with an MSI that works passively by collecting sunlight reflected from the Earth (https://sentinel.esa.int/web/sentinel/missions/sentinel-2/satellite-description). This instrument is responsible for measuring Earth's reflected radiance in 13 spectral bands (https://earth.esa.int/web/sentinel/technical-guides/sentinel-2-msi/msi-instrument).

The download of satellite images can be done through different platforms of equal capacity, but the one used in this work was EarthExplorer - a tool developed by the United States Geological Survey (USGS) (https://www.usgs.gov/earthexplorer-0). This platform allows us to filter images by location, period of time, satellite and percentage of cloud coverage present in the images, which should be the lowest value possible to reduce cloud interference. The images were downloaded from 2018 to 2020 and the match-ups made with the *in situ* sampling dates are presented in Table 2. Ideally, match-ups should not differ much in time; however, at the time of collection, samples were not carried out considering the availability of satellite imagery. The difference between most sampling dates and satellite imagery dates is due to either the imagery data available containing haze or cirrus clouds above the reservoirs or to the inability to perform water sampling at certain dates. Due to this, in one instance there were no images available to represent Autumn of 2019 in the Alqueva reservoir.

Table 2 - Match-ups between sampling dates and satellite imagery dates.

Reservoirs	Autumn 2018	Spring 2019	Autumn 2019	Spring 2020	Data source
Aguieira	5th-7th oct	6th apr	12th nov	10th may	**Sampling**
Aguieira	7th oct	21st mar	16th nov	29th may	**Satellite**
Alqueva	16th nov	15th may	18th nov	27th may	**Sampling**
Alqueva	22nd oct	5th may		29th may	**Satellite**

2.4 Image processing and parameter estimation

Several aspects must be considered when deriving water quality parameters from remotely sensed data. Optical sensors measure reflected light from the atmosphere and the surface of water bodies at visible (VIS) and near-infrared (NIR) wavelengths. However, around 90 % of the signal that reaches satellite sensors is affected by the absorption and scattering by different particles present in the atmosphere (e.g. water vapour, ozone, oxygen, carbon dioxide and aerosols) (Ansper & Alikas, 2019). This makes the use of AC processors fundamental in studies of this nature. AC processors can remove the scattered signal of the atmosphere and retrieve the signal from the water's surface (Matthews, 2011; Shanmugam, 2012). In this study the AC processor used was the Case 2 Regional Coast Colour (C2RCC). This processor relies on a database of radiative transfer simulations of water-leaving reflectance and Top-Of-Atmosphere (TOA) radiances. It is possible to apply this and other processors by using the Sentinel Application Platform (SNAP), a very useful tool jointly developed by Brockmann Consult, Skywatch and C-S.

Firstly, the downloaded images were loaded into SNAP and subsets that contained the reservoirs were created. These subsets are smaller in size than the original satellite images and were created so that the following processes require less computing power. After this, each image was resampled for different resolutions – 10 m, 20 m and 60 m. Afterward, the images were processed with C2RCC according to the default processing parameters, except for the neural nets setting which was changed to "C2X-Nets". Then, a Land/Sea mask was applied using a shapefile of each reservoir, making the file even smaller by reducing it to the Area of Interest (AOI). Finally, pins were loaded using the sampling point's coordinates and pixel values in those points were extracted.

Although it is possible to extract more information with the aid of C2RCC, the main outputs resulting from this work-flow were the bands "conc_chl" and "conc_tsm" - which stand for the parameters [Chl *a*] ($mg.m^{-3}$) and Total Suspended Matter concentration ([TSM]) ($g.m^{-3}$), respectively - and statistics from the sampling points concerning these bands (e.g. maximum, minimum and median values). A visual representation of the work-flow used can be seen in Fig. 4.

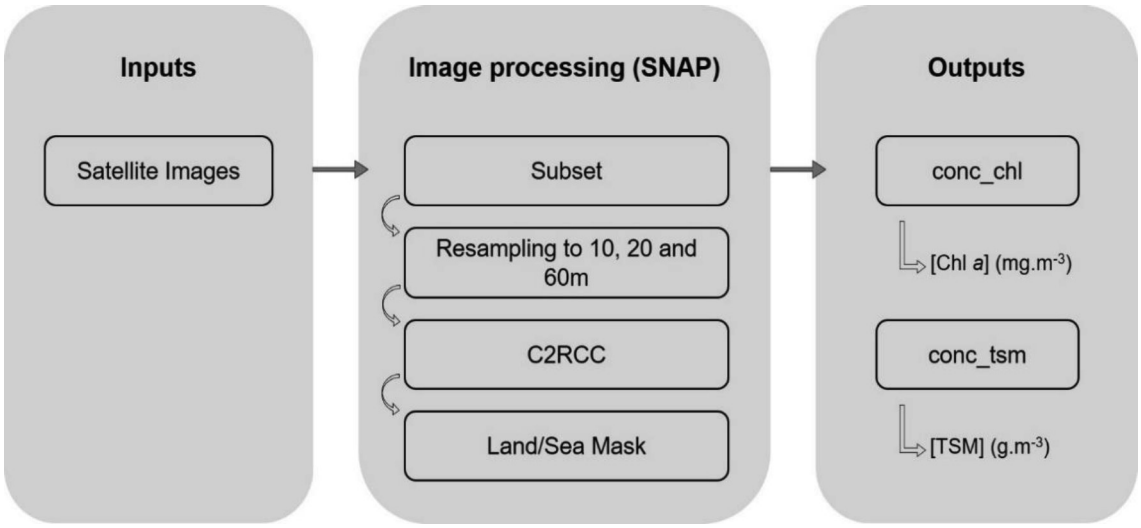

Fig. 4 - Workflow of image processing and parameter estimation.

2.5 Data analysis

Both reservoirs were analysed separately due to the inherent differences between inland water bodies. Firstly, some preliminary tests were performed. The normality of the distribution of satellite and *in situ* data was tested with Shapiro-Wilk tests to assess if parametric or non-parametric tests should be performed. These tests implied that, for both [Chl *a*] and [TSS/TSM] and both reservoirs, data distribution was significantly different from a normal distribution (p-value< 0.05). Therefore, parametric tests' assumptions are not met and the use of non-parametric tests is recommended. However, normality tests are often sensitive to sample size. For that purpose, Appendix I illustrates histograms of data distribution that were created to further corroborate the normality tests' results.

Secondly, a Kruskal-Wallis test was performed followed by a Pairwise Wilcoxon Rank Sum test to assess the statistical differences between all sites of each reservoir, concerning the parameters [Chl *a*] and [TSS].

The discrepancies between matching *in situ* data and all three resolutions of Sentinel-2 products (10 m, 20 m and 60 m) were evaluated using the following statistics: the Spearman's correlation coefficient, ρ (which does not assume a normal distribution of the data), the Normalized Root Mean Squared Error (NRMSE) and the Normalized Mean Bias Error (NMBE). The NRMSE (Equation 1) is a normalized measure of the relative error (scatter) and the NMBE (Equation 2) is the normalized average forecast error representing the systematic error of a forecast model to under or overforecast (Kato, 2016).

$$NRMSE(\%) = \frac{\sqrt{\frac{1}{N}\sum_{i=1}^{N}(Sat - Situ)^2}}{(Situ_{max} - Situ_{min})} \times 100 \quad (1)$$

$$NMBE(\%) = \frac{\frac{1}{N}\sum_{i=1}^{N}(Sat - Situ)}{(Situ_{max} - Situ_{min})} \times 100 \quad (2)$$

In both equations the terms Sat and Situ stand for the satellite and *in situ* data, respectively, and the terms $Situ_{max}$ and $Situ_{min}$ are the maximum and minimum values of *in situ* data.

Then, all data were transformed using a logarithmic (Log) function (log x + 1) and the *in situ* data and satellite estimates were plotted against each other. Statistical analysis of the *in situ* and satellite data, as well as the "match-ups" between both, was performed in *R* software. Results of the mentioned metrics and final graphs were also achieved using the *R* software (v3.6.1; {tdr} v0.13; {ggplot2} v3.2.1; {ggpubr} v0.4.0; {gtable} v0.3.0).

The last step in this study's methodology was to perform three different Principal Component Analysis (PCA). A first PCA was performed for the Aguieira reservoir using a matrix composed of physical-chemical parameters measured *in situ* and the parameters estimated via SNAP-C2RCC (*see* Appendix II, Table 8). A second PCA was performed for the Alqueva reservoir using a matrix composed of physical-chemical parameters measured *in situ* and the parameters estimated via SNAP-C2RCC (*see* Appendix II, Table 9). A final PCA was performed for both reservoirs using *in situ* parameters [Chl *a*] and Total Suspended Solids concentration ([TSS]) and their satellite "match-ups" (*see* Appendix II, Table 10). The variation within each dataset was assessed, as well as the Principal Component (PC) scores and Component Loading scores to better interpret each situation: PC scores inform about each observation and Loading scores inform about each variable.

PCAs were computed in order to reduce the dimensionality of the datasets, while retaining as much as possible of the variation present, making it easier to analyse the structure of the observations and the variables. The PCAs computed for the Aguieira and Alqueva reservoirs, separately, allow for the assessment of relations between physical and chemical parameters measured *in situ* and via satellite imagery, as well as the assessment of seasonal changes. The PCA computed for both reservoirs,

simultaneously, allows the assessment of the portability of the methodology applied for the two distinct reservoirs, in terms of the parameters [Chl *a*] and [TSS/TSM]. The direction and length of the arrows representing each variable can be visually interpreted as how much they contribute to the variation of data along a PC and numerically interpreted through the Loading scores for each PC. Results were obtained using the *R* software (v3.6.1; {ggbiplot} v0.55; {ggplot2} v3.2.1; {factoextra} v1.0.7).

3. Results

3.1 *In situ* data & SNAP-C2RCC estimates

All the results obtained through laboratory analysis of water samples and the processing of images using the C2RCC AC processor in SNAP are presented in Table 3.

For the Agueira reservoir, it was possible to obtain *in situ* and satellite data concerning the four sampling periods - Autumn of 2018 (Aut18), Spring of 2019 (Spr19), Autumn of 2019 (Aut19), and Spring of 2020 (Spr20).

For the Alqueva reservoir, it was possible to obtain *in situ* and satellite data concerning only three sampling periods - Autumn of 2018 (Aut18), Spring of 2019 (Spr19), and Spring of 2020 (Spr20). For Autumn 2019 it was not possible to obtain satellite imagery of the Alqueva reservoir close enough to the date when water samples were collected *in situ*, as previously mentioned (Table 2). This was due to all images available having considerable interference of either haze, cirrus and/or clouds. Therefore, no data concerning the season "Aut19" for the Alqueva reservoir is represented in Table 3 nor is used in statistical tests. All maps resulting from SNAP-C2RCC, concerning the bands "conc_chl" and "conc_tsm" are presented in Appendix III.

Table 3 - Results from laboratory analysis and Image processing using SNAP-C2RCC, concerning the Chl *a* and TSS/TSM parameters. "Chl *a*" is the Chlorophyll *a* measured *in situ* ($\mu g.L^{-1}$), "TSS" is the Total Suspended Solids measured *in situ* ($mg.L^{-1}$), "Chl-S10m", "Chl-S20m" and "Chl-S60m" are the SNAP-C2RCC estimated variables for Chlorophyll *a* ($\mu g.L^{-1}$), using the 10 m, 20 m, and 60 m products, respectively, and "TSM-S10m", "TSM-S20m" and "TSM-S60m" are the SNAP-C2RCC estimated variables for Total Suspended Matter ($mg.L^{-1}$), using the 10 m, 20 m, and 60 m products, respectively. The NA values occurred when the coordinates of a sampling point did not match a water-pixel in SNAP, likely due to the use of a lesser resolution (e.g. 60 m) or due to the decrease in water level in the reservoir leading to the emergence of the sampling point.

Season	Reservoir	Site	Chl *a*	Chl-S10m	Chl-S20m	Chl-S60m
Aut18	**Aguieira**	**A1**	5.429	15.979	13.524	6.640
Aut18	**Aguieira**	**A2**	10.096	0.080	0.021	9.973
Aut18	**Aguieira**	**A3**	1082.232	33.615	42.538	41.227
Aut18	**Aguieira**	**A4**	3.438	15.236	21.456	3.691
Spr19	**Aguieira**	**A1**	26.317	1.266	3.310	9.420
Spr19	**Aguieira**	**A2**	30.620	0.177	0.101	2.703
Spr19	**Aguieira**	**A3**	10.165	22.050	14.531	1.840
Spr19	**Aguieira**	**A4**	27.904	11.996	11.158	32.300

Season	Reservoir	Site	Chl *a*	Chl-S10m	Chl-S20m	Chl-S20m
Aut19	**Aguieira**	**A1**	1.610	0.931	1.336	1.278
Aut19	**Aguieira**	**A2**	2.590	0.198	0.319	0.626
Aut19	**Aguieira**	**A3**	10.960	57.304	22.514	33.832
Aut19	**Aguieira**	**A4**	5.300	0.301	0.299	NA
Spr20	**Aguieira**	**A1**	26.155	1.152	1.096	1.443
Spr20	**Aguieira**	**A2**	42.078	2.114	1.726	0.001
Spr20	**Aguieira**	**A3**	19.033	45.970	47.207	29.177
Spr20	**Aguieira**	**A4**	31.752	0.592	0.658	19.872
Aut18	**Alqueva**	**AI1**	0.98	11.446	12.72	16.028
Aut18	**Alqueva**	**AI2**	3.596	1.748	1.717	14.63
Aut18	**Alqueva**	**AI3**	1.812	12.824	12.832	10.78
Aut18	**Alqueva**	**AI4**	2.183	3.83E-04	3.76E-04	3.76E-04
Aut18	**Alqueva**	**AI5**	31.257	5.49E-03	8.71E-04	1.975
Spr19	**Alqueva**	**AI1**	2.285	NA	NA	NA
Spr19	**Alqueva**	**AI2**	0.936	1.818	0.105	0.003
Spr19	**Alqueva**	**AI3**	2.494	0.436	0.436	4.169
Spr19	**Alqueva**	**AI4**	7.832	3.73E-04	3.66E-04	3.66E-04
Spr19	**Alqueva**	**AI5**	56.649	0.858	0.585	2.567
Spr20	**Alqueva**	**AI1**	2.197	47.183	44.599	53.677
Spr20	**Alqueva**	**AI2**	2.281	12.53	13.498	22.423
Spr20	**Alqueva**	**AI3**	3.675	7.15E-04	7.26E-04	4.53E-04
Spr20	**Alqueva**	**AI4**	20.777	1.107	0.355	0.361
Spr20	**Alqueva**	**AI5**	45.419	38.058	31.452	1.217
Season	**Reservoir**	**Site**	**TSS**	**TSM-S10m**	**TSM-S20m**	**TSM-S60m**
Aut18	**Aguieira**	**A1**	8.24	21.456	21.63	6.869
Aut18	**Aguieira**	**A2**	10.09	0.166	0.138	7.551
Aut18	**Aguieira**	**A3**	312.5	70.421	77.763	83.318
Aut18	**Aguieira**	**A4**	10.75	6.329	10.129	0.303
Spr19	**Aguieira**	**A1**	13.45	10.922	10.154	19.06

Season	Reservoir	Site	TSS	TSM-S10m	TSM-S20m	TSM-S60m
Spr19	**Aguieira**	**A2**	19.05	0.091	0.145	8.201
Spr19	**Aguieira**	**A3**	11.08	31.514	26.155	0.5
Spr19	**Aguieira**	**A4**	17.5	0.815	0.763	207.936
Aut19	**Aguieira**	**A1**	7.82	1.889	1.244	2.922
Aut19	**Aguieira**	**A2**	10.75	0.05	0.045	0.167
Aut19	**Aguieira**	**A3**	12.58	124.712	70.101	49.608
Aut19	**Aguieira**	**A4**	5.55	0.035	0.035	NA
Spr20	**Aguieira**	**A1**	15.194	0.219	0.237	0.393
Spr20	**Aguieira**	**A2**	17.542	1.012	0.973	0.306
Spr20	**Aguieira**	**A3**	16.625	44.223	43.835	26.28
Spr20	**Aguieira**	**A4**	11.233	0.221	0.255	82.503
Aut18	**Alqueva**	**AI1**	4.28	65.274	56.571	62.241
Aut18	**Alqueva**	**AI2**	3.83	17.211	16.738	39.68
Aut18	**Alqueva**	**AI3**	4.72	35.153	35.132	31.673
Aut18	**Alqueva**	**AI4**	3.61	1.59	1.835	1.836
Aut18	**Alqueva**	**AI5**	15.42	11.742	10.515	13.666
Spr19	**Alqueva**	**AI1**	7.75	NA	NA	NA
Spr19	**Alqueva**	**AI2**	7.42	5.789	8.839	1.683
Spr19	**Alqueva**	**AI3**	7.42	3.78	3.78	17.354
Spr19	**Alqueva**	**AI4**	12.75	0.429	0.412	0.412
Spr19	**Alqueva**	**AI5**	20.42	0.798	0.62	9.208
Spr20	**Alqueva**	**AI1**	6.25	57.902	64.258	68.173
Spr20	**Alqueva**	**AI2**	7.083	21.194	21.105	21.541
Spr20	**Alqueva**	**AI3**	6.317	8.154	8.155	8.506
Spr20	**Alqueva**	**AI4**	10.021	7.601	7.473	7.467
Spr20	**Alqueva**	**AI5**	28.5	21.375	15.846	1.538

3.2 *In situ* data vs SNAP-C2RCC estimates

Kruskal-Wallis (Table 4) and Pairwise Wilcoxon Rank Sum (Table 5) tests' results revealed no significant differences between sampling points within each reservoir, concerning the Chl *a* and TSS *in situ* data (*p*-value> 0.05).

Table 4 – Results from Kruskal-Wallis tests for Aguieira and Alqueva considering *in situ* and satellite data of Chl *a* and TSS/TSM parameters.

Reservoir	Parameter	Chi-Squared	Degrees of freedom	*p*-value
Aguieira	**Chl *a***	0.99265	3	0.803
Alqueva	**Chl *a***	8.4333	4	0.07693
Aguieira	**TSS/TSM**	2.5018	3	0.475
Alqueva	**TSS/TSM**	7.2212	4	0.1246

Table 5 – Results from Pairwise Wilcoxon Rank Sum tests for Aguieira and Alqueva considering *in situ* data of Chl *a* and TSS/TSM parameters.

Reservoir	Parameter	Sampling Points	A1	A2	A3	
Aguieira	**Chl *a***	**A2**	*p*= 0.82			
Aguieira	**Chl *a***	**A3**	*p*= 0.82	*p*= 0.82		
Aguieira	**Chl *a***	**A4**	*p*= 0.82	*p*= 0.89	*p*= 0.82	
Aguieira	**TSS/TSM**	**A2**	*p*= 0.69			
Aguieira	**TSS/TSM**	**A3**	*p*= 0.69	*p*= 0.82		
Aguieira	**TSS/TSM**	**A4**	*p*= 1.00	*p*= 0.82	*p*= 0.69	
Reservoir	**Parameter**	**Sampling Points**	**A1**	**A2**	**A3**	**A4**
Alqueva	**Chl *a***	**A2**	*p*= 1.00			
Alqueva	**Chl *a***	**A3**	*p*= 0.50	*p*= 0.78		
Alqueva	**Chl *a***	**A4**	*p*= 0.50	*p*= 0.50	*p*= 0.50	
Alqueva	**Chl *a***	**A5**	*p*= 0.25	*p*= 0.25	*p*= 0.25	*p*= 0.25
Alqueva	**TSS/TSM**	**A2**	*p*= 1.00			
Alqueva	**TSS/TSM**	**A3**	*p*= 1.00	*p*= 1.00		
Alqueva	**TSS/TSM**	**A4**	*p*= 1.00	*p*= 1.00	*p*= 1.00	
Alqueva	**TSS/TSM**	**A5**	*p*= 0.25	*p*= 0.25	*p*= 0.25	*p*= 0.25

The results of Spearman's correlations are presented in Table 6. Regarding the [Chl *a*] in the Aguieira reservoir, a positive correlation between *in situ* and satellite data using 10 m, 20 m and 60 m products was recorded (ρ= 0.17, ρ= 0.14 and ρ= 0.35, respectively). Regarding [TSS/TSM], a positive correlation between *in situ* and satellite data using 10 m, 20 m, and 60 m products was also recorded (ρ= 0.25, ρ= 0.3 and ρ= 0.43, respectively). For the Alqueva reservoir, results of the Spearman's correlations for [Chl *a*] showed a negative correlation using 10 m, 20 m, and 60 m products (ρ= -0.28, ρ= -0.12 and ρ= -0.25, respectively). Regarding [TSS/TSM], a negative correlation using 10 m and 20 m products was also recorded in this reservoir

(ρ= -0.33 and ρ= -0.40, respectively). However, every result mentioned was not statistically significant (*p*-value> 0.05). The only significant result for Spearman's correlations was recorded in the Alqueva reservoir, for [TSS/TSM] using the 60 m product (ρ= -0.54, *p*-value< 0.05; Table 6), which indicates a modest but negative correlation (Fowler *et al.,* 1998).

Table 6 - Results of Spearman's Correlation for Aguieira and Alqueva reservoirs, considering *in situ* and satellite data of Chl *a* and TSS/TSM parameters.

Reservoir	Parameter	Chl-S10m	Chl-S20m	Chl-S60m
Aguieira	**Chl *a***	ρ= 0.170 *p*-value= 0.527	ρ= 0.140 *p*-value= 0.617	ρ= 0.350 *p*-value= 0.206
Alqueva	**Chl *a***	ρ= - 0.280 *p*-value= 0.325	ρ= - 0.120 *p*-value= 0.693	ρ= - 0.250 *p*-value= 0.391
		TSM-S10m	**TSM-S20m**	**TSM-S60m**
Aguieira	**TSS**	ρ= 0.250 *p*-value= 0.350	ρ= 0.300 *p*-value= 0.2537	ρ= 0.430 *p*-value= 0.109
Alqueva	**TSS**	ρ= - 0.330 *p*-value= 0.243	ρ= - 0.40 *p*-value= 0.151	**ρ= - 0.540** ***p*-value= 0.047**

To visualize the discrepancies between matching *in situ* and satellite data, along with the computation of NRMSE and NMBE, several plots were constructed. Fig. 5 is an example concerning the only instance where Spearman's correlation was statistically significant: for the Alqueva reservoir, using a 60 m product for [TSS/TSM]. The remaining plots are presented in Appendix IV. The results of the NRMSE and NMBE metrics are presented in Table 7.

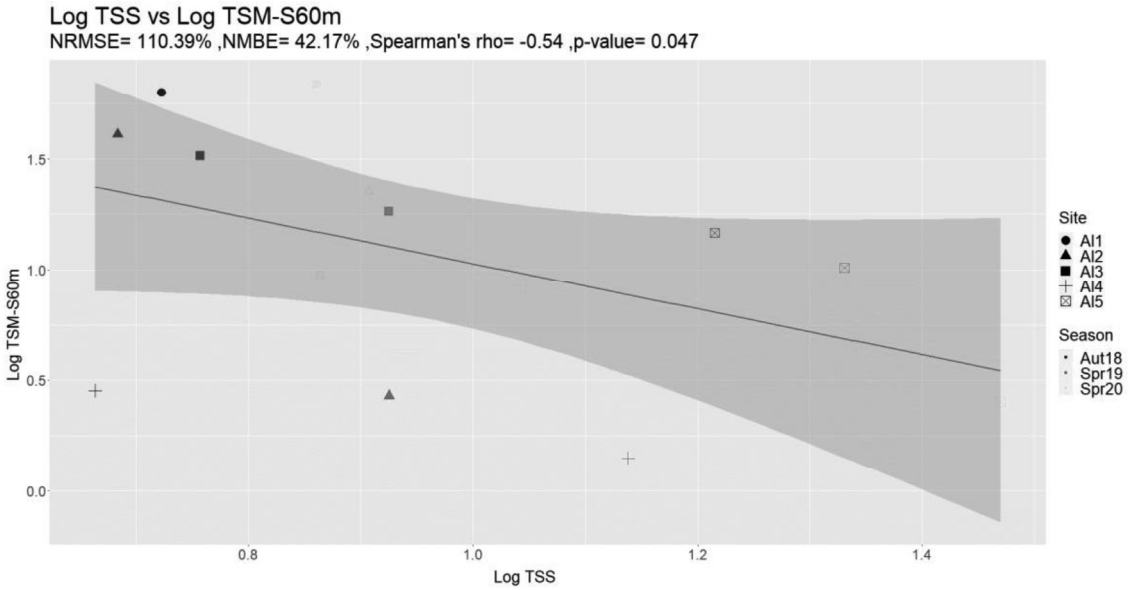

Fig. 5 - Alqueva reservoir; Log [TSM] from TSM-S60m plotted against Log [TSS] measured *in situ*.

Table 7 - NRMSE and NMBE results for Aguieira and Alqueva reservoir.

		10 m product		20 m product		60 m product	
		NRMSE	**NMBE**	**NRMSE**	**NMBE**	**NRMSE**	**NMBE**
Aguieira	**Chl *a***	24.35 %	-6.52 %	24.12 %	-6.67 %	24.92 %	-7.01 %
	TSS	22.17 %	-3.78 %	20.13 %	-4.81 %	26.11 %	0.03 %
Alqueva	**Chl *a***	40.07 %	-6.93 %	40.15 %	-8.18 %	47.30 %	-6.96 %
	TSS	97.96 %	34.42 %	96.60 %	32.23 %	110.39 %	42.17 %

Regarding [Chl *a*] results for the Aguieira reservoir (*see* Appendix IV Fig. 18, Fig. 19 and Fig. 20), most observations are aggregated between 0 and 2 for both datasets (*in situ* Log Chl *a* and satellite Log Chl *a*), the only exception was recorded for Aut18_A3 that has an *in situ* Log Chl *a* value of 3.035. NRMSE values were consistent across all resolutions - approximately 24 %, indicating some scatter of observations (relative error) (Table 7). In general, [Chl *a*] was slightly underestimated by SNAP-C2RCC for all resolutions, with Chl-S10m having the most accurate estimate values (NMBE = -6.52 %) (Table 7).

Regarding [TSS/TSM] results for the Aguieira reservoir (*see* Appendix IV Fig. 21, Fig. 22 and Fig. 23), most of the observations are aggregated between 0 and 2 for both values of Log TSS and Log TSM. Once again, Aut18_A3 was the only exception, presenting the highest Log TSS value (2.497). NRMSE results were more heterogeneous, with TSM-S20m allowing the least scatter of points (relative error)

(NRMSE = 20.11 %) (Table 7). TSM-S10m and TSM-S20m underestimated *in situ* TSS values by -3.78 % and -4.81 %, respectively. On the other hand, TSM-S60m almost perfectly predicted the *in situ* values (NMBE= 0.03 %) (Table 7).

Regarding [Chl *a*] results for the Alqueva reservoir (*see* Appendix IV Fig. 24, Fig. 25 and Fig. 26), observations aggregated between 0 and 2 for both *in situ* Log Chl *a* and satellite Log Chl *a* values. In this instance, NRMSE values were higher than seen in Aguieira, indicating a higher scatter of observations (relative error) (Table 7). NMBE results ranged between -8 % and -6 %, indicating an underestimation of *in situ* values by SNAP-C2RCC (Table 7).

Regarding [TSS/TSM] results for the Alqueva reservoir (Fig. 5 and *see* Appendix IV Fig. 27 and Fig. 28), observations are aggregated between 0 and 2 for both Log TSS and Log TSM values. NRMSE results were the highest recorded, ranging between 95 % and 110 % (Table 7), and NMBE results ranged between 32 % and 42 %, indicating that SNAP-C2RCC overestimated *in situ* values (high systematic error) (Table 7).

For assessing the distribution of observations in function of the physical and chemical water parameters measured *in situ* and estimated with SNAP-C2RCC, three PCAs were conducted (Fig. 6, Fig. 7 and Fig. 8). PCA for the Aguieira reservoir (Fig. 6), the Principal Component 1 (PC1) explains 35.8 % (eigenvalue= 11.46) of the variation in Aguieira's dataset while Principal Component 2 (PC2) explains 17.4 % of the variation (eigenvalue= 5.56), together explaining over than 50 % of the variation in the dataset. For this PCA, loading scores are presented in Appendix V Fig. 29, and PC scores are presented in Appendix VI Fig. 32.

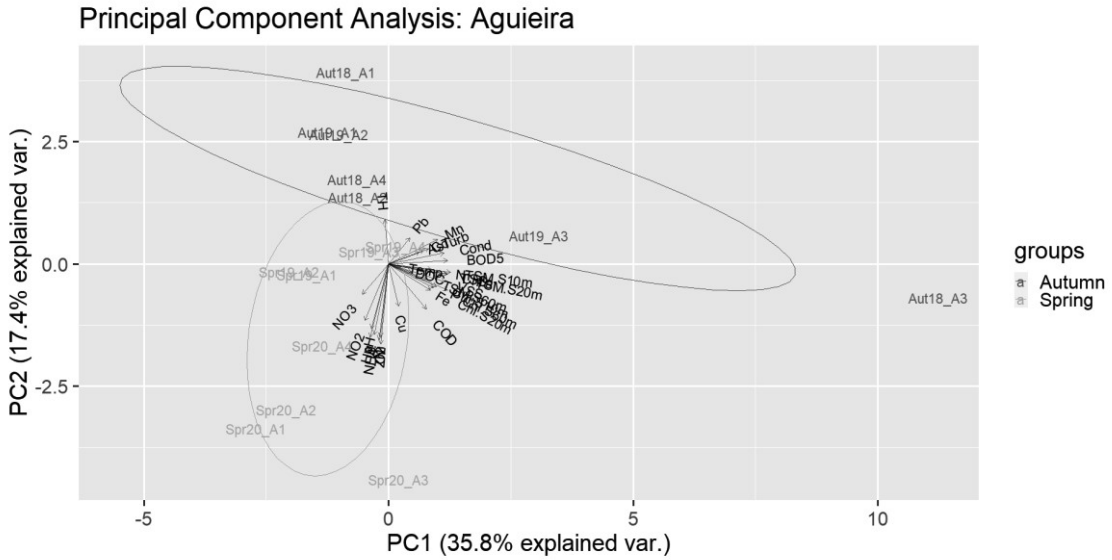

Fig. 6 – PCA for Aguieira reservoir. PC1 explains 35.8 % (eigenvalue= 11.46) of the variation in the dataset while PC2 explains 17.4 % of the variation (eigenvalue= 5.56).

According to the loading score results, most variables load positively onto PC1, with Kjedahl Nitrogen scoring the highest (Loading score= 0.285), followed by BOD_5 (Loading score= 0.271), Phosphorus (Loading score= 0.270), [TSS] (Loading score= 0.270) and [Chl *a*] (Loading score= 0.269). On the other hand, negative contributions were observed, namely associated with lowest scores of NO_3 (Loading score= -0.121) and NO_2 (Loading score= -0.108). Regarding the PC2, most variables load negatively, with TH loading the highest (Loading score= 0.202), while Zn loads the lowest (Loading score= -0.368) followed by Ni (Loading score= -0.347), Hg (Loading score= -0.338) and O_2 (Loading score= -0.336).

Two groups are represented by the ellipses; the blue ellipse represents Autumn observations and the green ellipse represents Spring observations. Some observations fall outside their groups – Aut18_A1, Aut18_A3, Spr20_A1 and Spr20_A3 - indicating that these observations are different than the remaining dataset. Therefore, given that Autumn and Spring observations differ mostly along PC2, TH is the variable that explains the distributions of Autumn observations, while Zn explains the dispersion recorded in Spring observations.

Indeed, according to the PC score results, Aut18_A3 scores the highest for PC1 (PC score= 11.231) while Spr20_A1 scores the lowest (PC score= -2.709) and Aut18_A1 scores the highest for PC2 (PC score= 3.912) while Spr20_A3 scores the lowest (PC score= -4.41). By knowing the loading scores of each variable, we can infer that

Aut18_A3's position is mostly explained by Kjedahl Nitrogen, while for Spr20_A1 it is NO_3, for Aut18_A1 it is TH and for Spr20_A3 it is Zn.

In the PCA for the Alqueva reservoir (Fig. 7), PC1 explains 36.1 % (eigenvalue= 11.56) of the variation in Alqueva's dataset and PC2 explains 27.9 % of the variation (eigenvalue= 8.83), together explaining over 60 % of the variation in the dataset. For this PCA, loading scores are presented in Appendix V Fig. 30, and PC scores are presented in Appendix VI Fig. 33.

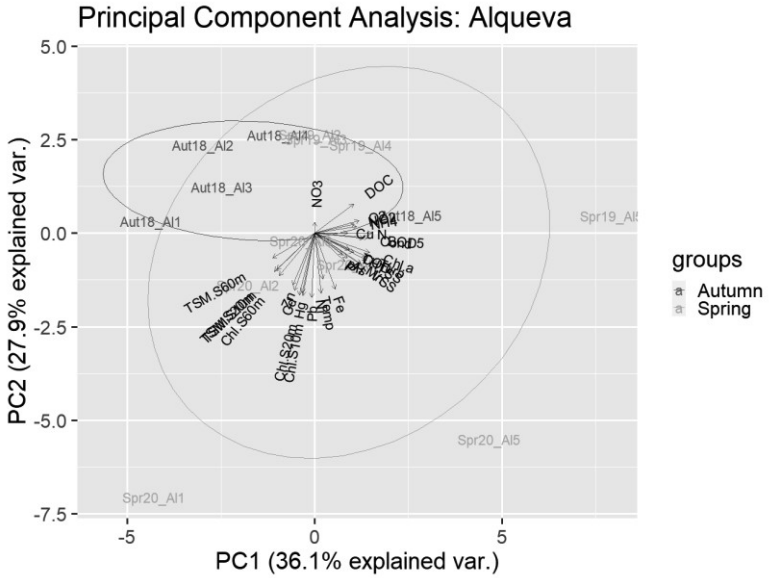

Fig. 7 - PCA for Alqueva reservoir. PC1 explains 36.1 % (eigenvalue= 11.56) of the variation in Alqueva's dataset and PC2 explains 27.9 % of the variation (eigenvalue= 8.83).

According to the loading score results, most variables load positively onto PC1, with Kjedahl Nitrogen loading the highest (Loading score= 0.277), followed by [Chl *a*] (Loading score= 0.264) and BOD_5 (Loading score= 0.261), while TSM-S60m loads the lowest (Loading score= -0.203), followed by TSM-S20m (Loading score= -0.193) and TSM-S10m (Loading score= -0.183). As for PC2, most variables load negatively, with DOC loading the highest (Loading score= 0.141) and Pb loading the lowest (Loading score= -0.311), followed by Chl-S10m (Loading score= -0.303) and Chl-S20m (Loading score= -0.299).

Two groups are formed; the blue ellipse represents Autumn observations and the green ellipse represents Spring observations. Some observations fall outside their groups – Aut18_Al1, Spr19_Al5, Spr20_Al1 and Spr20_Al5 -, once again, indicating that these observations are different than the remaining dataset. In this instance, seasonal differences are more ambiguous than in Aguieira reservoir due to the higher scatter of

observations. Therefore, it is not possible to infer confidently what variables are the most influencing for a given season.

As for PC score results, Spr19_Al5 scores the highest for PC1 (PC score= 7.936) followed by Spr20_Al5 (PC score= 4.655), while Aut18_Al1 scores the lowest (PC score= -4.364) followed by Spr20_Al1 (PC score= -4.286). As for PC2, positive contributions are low, with Spr19_Al2 scoring the highest (PC score= 2.644); however, negative contributions are more impactful, with Spr20_Al1 scoring the lowest (PC score= -7.048) followed by Spr20_Al5 (PC score= -5.514). By knowing the loading scores of each variable, we can infer that Spr19_Al5's position is mostly explained by Kjedahl Nitrogen, while for Spr20_Al5 it is both Kjedahl Nitrogen and Pb, for Aut18_Al1 it is TSM-S60m, for Spr20_Al1 it is TSM-S60m and Pb and for Spr19_Al2 it is DOC.

In the PCA for both reservoirs, accounting only for [Chl *a*] and [TSS/TSM] match-ups (Fig. 8), PC1 explains 60.6 % (eigenvalue= 4.85) of the variation in the dataset and PC2 explains 18.9 % of the variation (eigenvalue= 1.50), together explaining almost 80 % of the variation in the dataset. For this PCA, loading scores are presented in Appendix V Fig. 31 and PC scores are presented in Appendix VI Fig. 34.

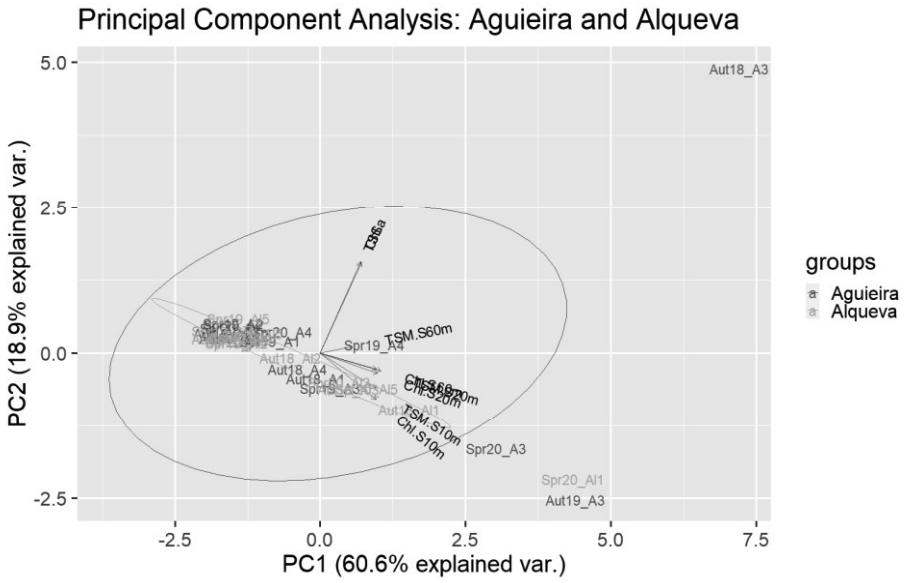

Fig. 8 – PCA for both reservoirs. PC1 explains 60.6 % (eigenvalue= 4.85) of the variation in the dataset and PC2 explains 18.9 % of the variation (eigenvalue= 1.50).

According to the loading score results, all variables load positively onto PC1 and are evenly distributed, with TSM-S20m loading the highest (Loading score= 0.421) and TSM-S60m loading the lowest (Loading score= 0.223). As for PC2, two variables stand out as positive loadings, [Chl *a*] loading the highest (Loading score= 0.633) followed by

[TSS] (Loading score= 0.626), and negative loadings were observed for Chl-S10m (Loading score= -0.318) and TSM-S10m (Loading score= -0.242).

Two groups are identified; the blue ellipse represents Aguieira reservoir observations and the green ellipse represents Alqueva reservoir observations. Some observations fall outside their groups – Aut18_A3, Aut19_A3, Spr20_A3,Spr19_Al5 and Spr20_Al1. In this situation, most observations from both reservoirs do not differ in position. However, it is visible that Aguieira has a much larger distribution that Alqueva. This is due to the contribution of both *in situ* variables, [Chl *a*] and [TSS], towards Aut18_A3 and of Chl-S10m and TSM-S10m towards Aut19_A3, Spr20_A3, and Spr20_Al1.

According to the PC score results, positive contributions to PC1 vary considerably, with Aut18_A3 scoring the highest (PC score= 7.205), followed by Aut19_A3 (PC score= 4.386) and Spr20_Al1 (PC score= 4.345). Negative contributions are mostly evenly distributed, with Aut18_Al4 scoring the lowest (PC score= -1.68) closely followed by Spr19_Al4 and Aut19_A2 (PC score= -1.675). As for PC2, Aut18_A3 stands out as a positive contribution (PC score= 4.886), with the remaining being evenly distributed, and as negative contributions Aut19_A3 scores the lowest (PC score= -2.522) followed by Spr20_Al1 (PC score= -2.174) and Spr20_A3 (PC score= -1.646).

4. Discussion

The present study aims to provide a practical complementary measure to fieldwork, that can be performed with high frequency at a comparatively low cost, across a spatially extensive area to assess water quality. In general, the results that support the methods used were obtained for the Aguieira reservoir. Below, these results are discussed along with other advantages associated with the use of satellite remote sensing technologies.

Data from NRMSE and NMBE metrics for Aguieira showed interesting results. For [Chl *a*] and [TSS/TSM], NRMSE results were around 20 %, indicating a slight scatter of observations (slight relative error). Considering the high sensitivity of this metric and the 4 observations outside the formed groups in Aguieira's PCA, results seem promising. NMBE results for [Chl *a*] indicated a slight underestimation of *in situ* data by SNAP-C2RCC, with values around 6-7 % (slight systematic error). In a study using Sentinel-3 OLCI imagery of lakes, Plowey (2019) achieved interesting statistics for [Chl *a*] retrieval (NMBE= -7 %, RMSE= 40 %, n=156), but high errors when retrieving [TSM] by using the standard C2RCC neural network. Kyryliuk and Kratzer (2019) demonstrated that [Chl *a*] was retrieved with a relatively low systematic error (NMBE= 10 %), but a high relative error (RMSE= 97 %, n=26). However, similarly to Plowey (2019), the authors observed a large systematic error (NMBE= 103 %) and an even larger relative error (RMSE= 167 %), when retrieving [TSM].

One of the most interesting results that came out of applying C2RCC to Sentinel-2 MSI data and comparing the results to *in situ* measurements was how well SNAP-C2RCC estimated [TSM] in the Aguieira reservoir. Despite using [TSM] as a proxy for [TSS] in this study, NMBE results are still very important, with an underestimation around 3-4 % using TSM-S10m and TSM-S20m and an almost perfect estimate using TSM-S60m (NMBE= 0.03 %). Results from the Aguieira PCA also show that the *in situ* and satellite data load similarly onto the PCs. These results indicate that the satellite data could be, in general, a good proxy for *in situ* data. However, it is important to keep in mind that the metrics used are normalized by the range of observed *in situ* data to allow for comparable results (Equation 1, *see* above Pag. 12)

Nowadays, there is an increasing regulatory need to expand the coverage and frequency of freshwater monitoring, arising from legislation such as the EU WFD. *In situ* monitoring is limited in terms of spatial coverage and representativeness, as well as the frequency for many sites, and is simply non-existent in many others (Palmer *et al.,* 2015). Remote sensing can provide a suitable means to integrate limnological data collected from traditional *in situ* measurements, with the advantages of good spatial and temporal

coverage and the possibility of measuring several water bodies, simultaneously (Koponen *et al.,* 2002; Ritchie *et al.,* 1990). Hyperspectral sensing is capable of producing more and narrower bands than the MSI used in Sentinel-2. It offers the potential to detect water quality variables by using narrow spectral channels, which would otherwise be masked by satellites with broader bands. Therefore, many researchers expect it to become a standard technology for measuring water quality parameters such as [Chl *a*] (Richardson, 1996; Schmidt & Skidmore, 2001). Although the methods to retrieve water quality information from remote sense data might not be as precise as traditional methods at the moment, they are time and cost efficient over a large area and can provide the opportunity for regular observation even of remote regions (Hadjimitsis & Clayton, 2009; Seker *et al.,* 2003).

Inland water remote sensing has faced, and continues to face, many challenges not only in terms of the science underpinning the retrieval of physical and biogeochemical properties over typically highly optically complex waters, but it has also suffered from lack of funding, infrastructure and the mechanisms needed to coordinate research efforts across an historically fragmented community (Palmer *et al.,* 2015). This has meant that the inland water community has often had to make use of data from satellite sensors designed primarily for land applications. While these sensors have adequate spatial resolutions for some water bodies their spectral coverage and resolution are not optimal for many applications over inland waters (e.g. CDOM retrieval). The optical complexity of inland waters, AC issues and adjacency effects add additional challenges to inland water remote sensing (Palmer *et al.,* 2015).

Regarding the process of AC, Pereira-Sandoval *et al.* (2019) studied the most appropriate AC processor to be applied to Sentinel-2 MSI Imagery over several types of inland waters in Valencia, Spain, including eight reservoirs and a coastal lagoon. Statistical linear analysis showed that Polymer and C2RCC were the processors with the highest correlation coefficients and lowest errors when comparing *in situ* measurements and satellite reflectance. They concluded that due to the results obtained for both these AC processors it was possible to support the applicability of Sentinel-2 MSI for inland water quality estimation. Due to its inclusion in SNAP, its simple interface and the representative results achieved in other studies, C2RCC was chosen as the AC processor in our study. However, the processing parameters were kept by default except for the neural net, which was changed to “C2X-Nets” - appropriate for extreme Case-2 Waters. Taking into account the observation of very eutrophicated sampling points, such as Aut18_A3 (Chl *a*= 1082.232 µg.L^{-1}) and Spr19_Al5 (Chl *a*= 56.649 µg.L^{-1}), as well as

the good results achieved with its use by Soomets *et al.* (2020), we decided to apply this neural net.

The optical properties of inland waters are highly variable between and even within water bodies. These issues confound the development of algorithms for inland waters and typically limit their applicability to different water bodies (Palmer *et al.,* 2015). For example, Johansen *et al.* (2018) evaluated the performances of 29 algorithms that use satellite-based spectral imager data to derive estimates of [Chl *a*] that, in turn, can be used as an indicator of the general status of algal cell densities and the potential for CHABs. Their purpose was to identify algorithm-imager combinations that had a high correlation with coincident [Chl *a*] surface observations for two temperate inland lakes, as it suggested portability for regional CHAB monitoring. Even though the two lakes were different in terms of background water quality, size and shape, the results obtained support the portability of utilizing a suite of certain algorithms across multiple sensors to detect potential algal blooms through the use of [Chl *a*] as a proxy.

In this study we also aim to assess the portability of the application of the C2RCC processing chain between the reservoirs studied. For this purpose, we should consider the PCA of both reservoirs, which uses *in situ* and satellite results of [Chl *a*] and [TSS/TSM]. Regarding the PCA of both reservoirs (Fig. 8) it is possible to observe, through the formed groups, that Alqueva observations are more associated than Aguieira observations, i.e. there is less variation within Alqueva observations than Aguieira observations. It is also possible to observe differences between *in situ* and satellite variables, given that their respective parameters are placed almost perpendicularly in the PCA biplot.

Using Aut18_A3 as an example, the values measured *in situ* and estimated through SNAP-C2RCC are very distinct: while *in situ* [Chl *a*] measured was 1082.232 $\mu g.L^{-1}$ the satellite estimates were around 30-40 $\mu g.L^{-1}$, and while *in situ* [TSS] measured was 312.5 $mg.L^{-1}$ the satellite estimates were around 70-80 $mg.L^{-1}$. A possible explanation may concern image processing. Sampling points such as A3 in Aguieira are characterized by usually being very eutrophicated areas. Kyryliuk and Kratzer (2019) found that at very high CDOM absorption, observed at some sites in their AOI, the remote sensing reflectance was generally reduced. Kratzer and Vinterhav (2010) showed that Case 2 Regional (C2R) - a previous version of C2RCC - had a problem in which the AC seemed to overcorrect the atmospheric influence. It is possible that the AC used by C2RCC in this study may have also overcompensated for the negative reflectances that often occur in waters with relatively high CDOM absorption (Fan *et al.,* 2017). In turn,

this would have caused the estimates of SNAP-C2RCC to not be as reliable in very eutrophicated sampling points.

Also, Toming *et al.,* 2017 tested the performance of the standard C2RCC processing chain in retrieving water reflectance, inherent optical properties (IOPs), and water quality parameters such as [Chl *a*], [TSM] and CDOM in the Baltic Sea. The Baltic Sea, just like reservoirs, is an optically complex water body where many ocean colour products, performing well in other water bodies, fail. The authors observed that, although the reflectance spectra produced by the C2RCC are realistic in both shape and magnitude, the IOPs (and consequently the water quality parameters) estimated by C2RCC did not correlate with the *in situ* data. A parallel can be drawn with our study, given that the Spearman's correlation results between *in situ* measurements and satellite estimates were mostly not significant. However, the authors also observed that some tested empirical remote sensing algorithms performed well in retrieving [Chl *a*], [TSM], CDOM and Secchi depth from the reflectance produced by the C2RCC. This suggest that the AC part of the processor performs relatively well while the IOP retrieval part needs extensive training with the actual IOP data before it can produce reasonable estimates for a given AOI.

IOPs vary not only across geographic regions but also within the same water mass (Mishra *et al.,* 2017). The complexity of the reservoirs is mainly due to the spatial-temporal variability of the water constituents at the same site. In other words, the dominant constituent in the water column at a study site may not only change spatially across short distances but also seasons (Huang *et al.,* 2015; Yacobi *et al.,* 1995). Aguieira PCA (Fig. 6) results for Spring and Autumn are different. It is visible by the groups formed that, while Autumn observations are more dispersed, Spring observations are closer despite still having observations outside the group. On one hand, Autumn observations are mainly explained by the TH variable. On the other hand, Spring observations are mainly explained by metals such as Zn, Ni and Hg, and contaminants such as Nitrites and Nitrates. In Alqueva PCA, results for the two seasons are similar. Here, there is an inverse situation to the Aguieira PCA: Autumn observations are more grouped and Spring observations are more dispersed, mainly due to the positions of Spr19_Al5, Spr20_Al1, and Spr20_Al5. In this reservoir, seasonal changes are more ambiguous and, therefore, no specific variables were identified that influence Autumn and Spring observations.

Neiva, Antunes, Carvalho, & Santos (2016) studied an abandoned Mondego Sul uranium mine, located in between sampling points A1 and A4 in Aguieira. The area occupied by the mine site extended for 400 m and is within the protected area of the

reservoir. They indicated the existence of five open pits and observed that drainage water was running to the reservoir from dumps. The largest of the dumps is located close to the reservoir, with a spring at the bottom. The authors reported that the highest contaminations in Ni occurred in the Spring, due to the highest flow. Also, they confirmed that median values of metals of stream sediments were higher than those of European stream sediments. Therefore, they significantly affected the composition of waters in the confluence with the Mondego river, including the Aguieira reservoir. The influence of this abandoned mine site over the reservoir seems to be the reason behind the seasonal behaviour of the variables. As the authors concluded, the water, stream sediment and soil from the whole area must be remediated.

Notwithstanding, it seems that seasonal changes are more notorious in Aguieira than in Alqueva. However, it is important to note that these differences are not caused by the satellite data in the dataset, but mostly by the physical and chemical parameters measured. In other words, seasonal changes seem to be independent of the use of satellite estimated data. It is also very important to note that differences between sampling points seemed to have more impact than differences concerning the seasons, i.e. spatial differences seem more impactful than temporal differences.

Nevertheless, the temporal dimension should always be considered, particularly when discussing the dates when the samplings are performed compared to the dates when the satellite images are captured. As mentioned before, in this study this aspect was not possible to control given that the study started after all samplings had been made, as a part of a different goal of project ReDEFine. It is very important to consider the functions performed by the reservoirs in question. Among reservoirs, those built for generating hydroelectricity usually have the most pronounced fluctuations in water level. These fluctuations result from variations in the electricity demand (Nilsson, 2013). Also, reservoirs built for water storage aim to sustain flow in the river downstream and level out ordinary fluctuations in discharge (Nilsson, 2013). The Aguieira and Alqueva reservoirs were built for these functions.

Fig. 9 represents the monthly mean storage volume in each reservoir for the last two water years (2018-2019 and 2019-2020). An evident temporal variation of the shape and size of both reservoirs is recorded. Therefore, given the regular changes that occur in a reservoir, it is ideal to collect samples on the same day when satellite images will capture the reservoir. Kyryliuk and Kratzer (2019) were able to plan this aspect in their work. They used the weather app “Weather Pro” to screen, with 7-day forecasting, for cloud-free dates closer to the “overpass” time of the satellite over their study area. The

European Space Agency (ESA) also provides a tool that allows to predict the "overpass" time of a satellite over an AOI (https://evdc.esa.int/orbit/).

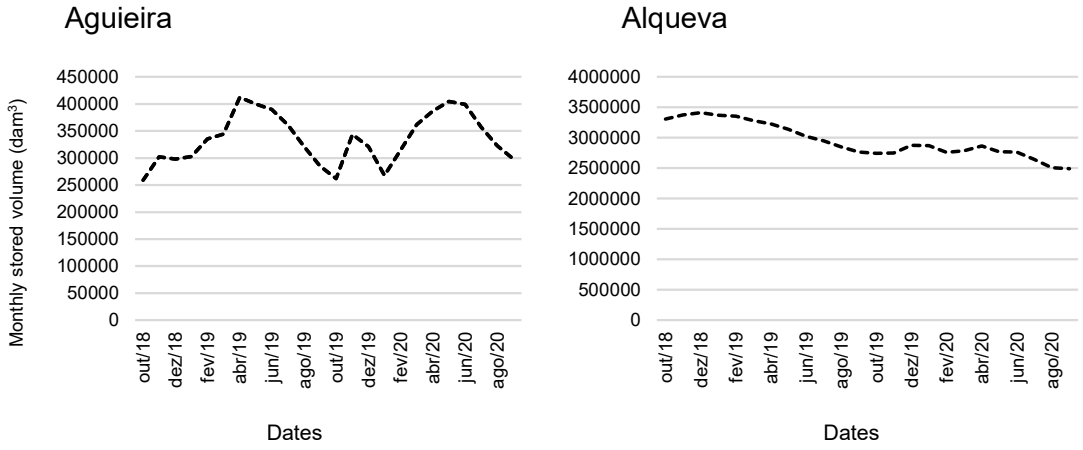

Fig. 9 - Monthly mean stored volume of water in Aguieira reservoir (left) and Alqueva Reservoir (right), for the last two water years (2018-2019 ad 2019-2020).

Particularly in cloudier seasons such as Autumn and Winter, there is less availability of suitable satellite images - i.e. images with no cloud, haze or cirrus interference and that capture the reservoir in its entirety. If the field campaign to retrieve water samples is not planned considering the "overpass" of the satellite over the AOI, there may not be suitable images to match with *in situ* data. In turn, this will affect the accuracy of the results, or even impede the study altogether. In conclusion, ideally the dates should be the same for both retrievals because the availability of suitable satellite imagery can be a limiting factor when not considered beforehand.

The inland water community is smaller in number, more fragmented and less well funded than the ocean colour community, particularly when one considers the number and complexity of the challenges currently faced. In general, the wider scientific community has been slow to fully recognise the importance of freshwater ecosystems to global-scale processes and the provisioning of ecosystem services upon which human society relies (Palmer *et al.,* 2015). Although inland waters comprise a small fraction of the Earth's surface water, it is becoming increasingly clear that they are of disproportionate importance to the global biosphere (Downing, 2014). Despite a large amount of valuable inland water remote sensing research having been overlooked because it was either published in the pre-digital era or in the grey literature - i.e. conference proceedings, PhD thesis, etc. – the current advancements in this field of study have marked improvements in the accuracy, applicability and robustness of remote sensing products for inland waters (Palmer *et al.,* 2015). By studying the validity of

applying C2RCC to these two reservoirs we hope not only to contribute to these improvements, but also bring forth new knowledge concerning inland waters, and particularly reservoirs.

It is immensely encouraging that in the last few years, several large projects on remote sensing of inland waters have been funded (particularly within the EU), including: the ESA Diversity II project (http://www.diversity2.info) and the EC FP7 eartH2Observe project (http://www.earth2observe.eu). The funding of projects such as these is fundamental for the collective growth and improvement of the limnology and remote sensing communities, as satellite remote sensing has been proven to be a low-cost and rapid alternative to monitor water quality.

In a direct follow-up to this study it would be compelling to explore some aspects. Firstly, it would be interesting to apply a different AC processor to the Alqueva reservoir. This way, it would be possible to assess if the lesser results obtained in this study were due to the use of C2RCC in this water body, or due to some other reason. Secondly, it could be of interest to study the Aguieira reservoir with more detail. Ideally, new water samples would be collected on the same day as satellite images are captured. Also, alongside them, water column reflectances would be measured, allowing for two different measures to be compared with traditionally collected data. In addition, more details regarding C2RCC processing parameters should be gathered to allow for more precise results.

Finally, it is advisable for the EU to aim to implement monitoring protocols that use these technologies, in the future. As proven by this study, two different water masses may respond with different degrees of success to the same methodology. In order to fully take advantage of such useful technologies, it is important to invest time and resources as soon as possible, because studying the most reliable way to assess several water bodies may take some time.

5. References

Ansper, A., & Alikas, K. (2019). Retrieval of chlorophyll a from Sentinel-2 MSI data for the European Union water framework directive reporting purposes. Remote Sensing, 11(1), 64. https://doi.org/10.3390/rs11010064

APHA. (1989). Standard Methods for the Examination of Water and Wastewater. In American Public Health Association (17th ed.).

Blabolil, P., Logez, M., Ricard, D., Prchalová, M., Říha, M., Sagouis, A., Peterka, J., Kubečka, J., & Argillier, C. (2016). An assessment of the ecological potential of Central and Western European reservoirs based on fish communities. Fisheries Research, 173, 80–87. https://doi.org/10.1016/j.fishres.2015.05.022

Corman, J. (2017). Aquatic biogeochemistry: Cleaner Chinese lakes. Nature Geoscience, 10, 469–470. https://doi.org/10.1038/ngeo2977

Corrigan, J. R., Egan, K. J., & Downing, J. A. (2009). Aesthetic Values of Lakes and Rivers. In Encyclopedia of Inland Waters. Elsevier Inc. https://doi.org/10.1016/B978-012370626-3.00003-X

De Figueiredo, D. R., Azeiteiro, U. M., Esteves, S. M., Gonçalves, F. J. M., & Pereira, M. J. (2004). Microcystin-producing blooms—a serious global public health issue. Ecotoxicology and Environmental Safety, 59(2), 151–163. https://doi.org/10.1016/J.ECOENV.2004.04.006

Downing, J. A. (2014). Limnology and oceanography: Two estranged twins reuniting by global change. Inland Waters, 4(2), 215–232. https://doi.org/10.5268/IW-4.2.753

Duan, H., Ma, R., Xu, J., Zhang, Y., & Zhang, B. (2010). Comparison of different semi-empirical algorithms to estimate chlorophyll-a concentration in inland lake water. Environmental Monitoring and Assessment, 170, 231-244. https://doi.org/10.1007/s10661-009-1228-7

European Community. (2000). Directive 2000/60/EC of the European Parliament and of the Council of 23 October 2000 establishing a framework for Community action in the field of water policy. Official Journal of the European Parliament. https://doi.org/10.1039/ap9842100196

Fan, Y., Li, W., Gatebe, C. K., Jamet, C., Zibordi, G., Schroeder, T., & Stamnes, K. (2017). Atmospheric correction over coastal waters using multilayer neural networks. Remote Sensing of Environment, 199, 218–240. https://doi.org/10.1016/j.rse.2017.07.016

Fowler, J., Cohen, L., & Jarvis, P. (1998). Pratical statics for Field biology. In Wiley Editorial Offices (2nd ed.). John Wiley & Sons Ltd.

Giardino, C., Bresciani, M., Stroppiana, D., Oggioni, A., & Morabito, G. (2014). Optical remote sensing of lakes: An overview on Lake Maggiore. Journal of Limnology, 73(s1). https://doi.org/10.4081/jlimnol.2014.817

Gordon, H. R. (1988). A semianalytic radiance model of ocean color. Journal of Geophysical Research, 93(D9), 10909–10924. https://doi.org/10.1029/JD093iD09p10909

Hadjimitsis, D. G., & Clayton, C. (2009). Assessment of temporal variations of water quality in inland water bodies using atmospheric corrected satellite remotely sensed image data. Environmental Monitoring and Assessment, 159, 281-292. https://doi.org/10.1007/s10661-008-0629-3

Han, J. H., Kim, B., Kim, C., & An, K. G. (2014). Ecosystem health evaluation of agricultural reservoirs using multi-metric lentic ecosystem health assessment (LEHA) model. Paddy and Water Environment, 12(SUPPL1), 7–18. https://doi.org/10.1007/s10333-014-0444-0

Huang, C., Shi, K., Yang, H., Li, Y., Zhu, A. X., Sun, D., Xu, L., Zou, J., & Chen, X. (2015). Satellite observation of hourly dynamic characteristics of algae with Geostationary Ocean Color Imager (GOCI) data in Lake Taihu. Remote Sensing of Environment, 159, 278–287. https://doi.org/10.1016/j.rse.2014.12.016

Hudnell, H. K., Dortch, Q., & Zenick, H. (2008). An overview of the interagency, International Symposium on Cyanobacterial Harmful Algal Blooms (ISOC-HAB): advancing the scientific understanding of freshwater harmful algal blooms. Advances in Experimental Medicine and Biology, 619, 1–16. https://doi.org/10.1007/978-0-387-75865-7_1

Irz, P., Laurent, A., Messad, S., Pronier, O., & Argillier, C. (2002). Influence of site characteristics on fish community patterns in French reservoirs. Ecology of Freshwater Fish, 11(2), 123-136. https://doi.org/10.1034/j.1600-0633.2002.00004.x

Jennings, M. J., Fore, L. S., & Karr, J. R. (1995). Biological monitoring of fish assemblages in Tennessee Valley reservoirs. Regulated Rivers: Research & Management, 11(3–4), 263–274. https://doi.org/10.1002/rrr.3450110303

Johansen, R., Beck, R., Nowosad, J., Nietch, C., Xu, M., Shu, S., Yang, B., Liu, H., Emery, E., Reif, M., Harwood, J., Young, J., Macke, D., Martin, M., Stillings, G., Stumpf, R., & Su, H. (2018). Evaluating the portability of satellite derived chlorophyll-a algorithms for temperate inland lakes using airborne hyperspectral imagery and dense surface observations. Harmful Algae, 76, 35–46. https://doi.org/10.1016/j.hal.2018.05.001

Kato, T. (2016). Prediction of photovoltaic power generation output and network operation. In Integration of Distributed Energy Resources in Power Systems: Implementation, Operation and Control. Elsevier Inc. https://doi.org/10.1016/B978-0-12-803212-1.00004-0

Kirk, K. L., & Gilbert, J. J. (1992). Variation in herbivore response to chemical defenses: zooplankton foraging on toxic cyanobacteria. Ecology, 73(6), 2208–2217. https://doi.org/10.2307/1941468

Koponen, S., Pulliainen, J., Kallio, K., & Hallikainen, M. (2002). Lake water quality classification with airborne hyperspectral spectrometer and simulated MERIS data. Remote Sensing of Environment, 79(1), 51–59. https://doi.org/10.1016/S0034-4257(01)00238-3

Kratzer, S., & Vinterhav, C. (2010). Improvement of MERIS level 2 products in baltic sea coastal areas by applying the improved Contrast between Ocean and Land Processor (ICOL) - Data analysis and validation. Oceanologia, 52(2), 211–236. https://doi.org/10.5697/oc.52-2.211

Kyryliuk, D., & Kratzer, S. (2019). Evaluation of sentinel-3A OLCI products derived using the case-2 regional coastcolour processor over the Baltic Sea. Sensors (Switzerland), 19(16). https://doi.org/10.3390/s19163609

Lorenzen, C. J. (1967). Determination of Chlorophyll and Pheo-Pigments: Spectrophotometric Equations. Limnology and Oceanography, 12(2), 343–346. https://doi.org/10.4319/lo.1967.12.2.0343

Matthews, M. W. (2011). A current review of empirical procedures of remote sensing in Inland and near-coastal transitional waters. International Journal of Remote Sensing, 32(21), 6855-6899. https://doi.org/10.1080/01431161.2010.512947

Merel, S., Walker, D., Chicana, R., Snyder, S., Baurès, E., & Thomas, O. (2013). State of knowledge and concerns on cyanobacterial blooms and cyanotoxins. Environment International, 59, 303–327. https://doi.org/10.1016/J.ENVINT.2013.06.013

Mishra, D. R., Ogashawara, I., & Gitelson, A. A. (2017). Bio-optical Modeling and Remote Sensing of Inland Waters. Bio-optical Modeling and Remote Sensing of Inland Waters. Elsevier Inc.

Morel, A. Y., & Gordon, H. R. (1980). Report of the working group on water color. Boundary-Layer Meteorology, 18, 343–355. https://doi.org/10.1007/BF00122030

Müller-Navarra, D. C., Brett, M. T., Liston, A. M., & Goldman, C. R. (2000). A highly unsaturated fatty acid predicts carbon transfer between primary producers and consumers. Nature, 403(6765), 74–77. https://doi.org/10.1038/47469

Navarro, E., Caputo, L., Marcé, R., Carol, J., Benejam, L., Garcia-Berthou, E., & Armengol, J. (2009). Ecological classification of a set of Mediterranean reservoirs applying the EU Water Framework Directive: A reasonable compromise between science and management. Lake and Reservoir Management, 25(4), 364–376. https://doi.org/10.1080/07438140903238567

Neiva, A. M. R., Antunes, I. M. H. R., Carvalho, P. C. S., & Santos, A. C. T. (2016). Uranium and arsenic contamination in the former Mondego Sul uranium mine area, Central Portugal. Journal of Geochemical Exploration, 162, 1–15. https://doi.org/10.1016/j.gexplo.2015.12.004

Nilsson, C. (2013). Reservoirs. Reference Module in Earth Systems and Environmental Sciences. https://doi.org/10.1016/B978-0-12-409548-9.03881-1

Paerl, H. W., & Huisman, J. (2008). Blooms like it hot. Science (New York, N.Y.), 320(5872), 57–58. https://doi.org/10.1126/science.1155398

Palmer, S. C. J., Kutser, T., & Hunter, P. D. (2015). Remote sensing of inland waters: Challenges, progress and future directions. Remote Sensing of Environment, 157, 1–8. https://doi.org/10.1016/j.rse.2014.09.021

Pekel, J. F., Cottam, A., Gorelick, N., & Belward, A. S. (2016). High-resolution mapping of global surface water and its long-term changes. Nature, 540(7633), 418–422. https://doi.org/10.1038/nature20584

Pereira-Sandoval, M., Ruescas, A., Urrego, P., Ruiz-Verdú, A., Delegido, J., Tenjo, C., Soria-Perpinyà, X., Vicente, E., Soria, J., & Moreno, J. (2019). Evaluation of atmospheric correction algorithms over spanish inland waters for sentinel-2 multi spectral imagery data. Remote Sensing, 11(12), 1–23. https://doi.org/10.3390/rs11121469

Plowey, M. (2019). A Multi-Scale Approach to Monitoring the Optically Complex Coastal Waters of the Baltic Sea - A comparison of Satellite, Mooring, and Ship-based Monitoring of Ocean Colour. Stockholm University.

Potes, M., Rodrigues, G., Marchã Penha, A., Helena Novais, M., João Costa, M., Salgado, R., & Manuela Morais, M. (2018). Use of Sentinel 2-MSI for water quality monitoring at Alqueva reservoir, Portugal. Proceedings of the International Association of Hydrological Sciences, 380 (December), 73–79. https://doi.org/10.5194/piahs-380-73-2018

Qin, B., Xu, P., Wu, Q., Luo, L., & Zhang, Y. (2007). Environmental issues of Lake Taihu, China. Hydrobiologia, 581, 3-14. https://doi.org/10.1007/s10750-006-0521-5

Richardson, L. L. (1996). Remote sensing of algal bloom dynamics. BioScience, 46(7), 492-501. https://doi.org/10.2307/1312927

Ritchie, J. C., Cooper, C. M., & Schiebe, F. R. (1990). The relationship of MSS and TM digital data with suspended sediments, chlorophyll, and temperature in Moon Lake, Mississippi. Remote Sensing of Environment, 33(2), 137–148. https://doi.org/10.1016/0034-4257(90)90039-O

Scheffer, M., & Carpenter, S. R. (2003). Catastrophic regime shifts in ecosystems: linking theory to observation. Trends in Ecology & Evolution, 18(12), 648–656. https://doi.org/10.1016/J.TREE.2003.09.002

Schmidt, K. S., & Skidmore, A. K. (2001). Exploring spectral discrimination of grass species in African rangelands. International Journal of Remote Sensing, 22(17), 3421–3434. https://doi.org/10.1080/01431160152609245

Seker, D. Z., Goksel, C., Kabdasli, S., Musaoglu, N., & Kaya, S. (2003). Investigation of coastal morphological changes due to river basin characteristics by means of remote sensing and GIS techniques. Water Science and Technology, 48(10), 135–142. https://doi.org/10.2166/wst.2003.0558

Shanmugam, P. (2012). CAAS: An atmospheric correction algorithm for the remote sensing of complex waters. Annales Geophysicae, 30, 203-220. https://doi.org/10.5194/angeo-30-203-2012

Soomets, T., Uudeberg, K., Jakovels, D., Brauns, A., Zagars, M., & Kutser, T. (2020). Validation and comparison of water quality products in baltic lakes using sentinel-2 msi and sentinel-3 OLCI data. Sensors (Switzerland), 20(3), 742. https://doi.org/10.3390/s20030742

Sòria-Perpinyà, X., Urrego, P., Pereira-Sandoval, M., Ruiz-Verdú, A., Peña, R., Soria, J. M., Delegido, J., Vicente, E., & Moreno, J. (2019). Monitoring the ecological state of a hypertrophic lake (Albufera of València, Spain) using multitemporal sentinel-2 images. Limnetica, 38(1), 457–469. https://doi.org/10.23818/limn.38.26

Soria, X., Delegido, J., Urrego, E., Pereira, M., Vicente, E., Ruiz, A., Soria, J., Peña, R., C, T., & Moreno, J. (2017). Validación de algoritmos para la estimación de la Clorofila- a con Sentinel-2 en la Albufera de Valencia. Nuevas Plataformas y Sensores de Teledetección, 3(7), 289–292.

Toming, K., Kutser, T., Uiboupin, R., Arikas, A., Vahter, K., & Paavel, B. (2017). Mapping water quality parameters with Sentinel-3 Ocean and Land Colour Instrument imagery in the Baltic Sea. Remote Sensing, 9(10). https://doi.org/10.3390/rs9101070

Visser, P. M., Ibelings, B. W., Mur, L. R., & Walsby, A. E. (2005). The Ecophysiology of the Harmful Cyanobacterium Microcystis. Harmful Cyanobacteria. Springer, Dordrecht. https://doi.org/10.1007/1-4020-3022-3_6

Wetzel, R. G. (2001). Limnology: Lake and River Ecosystems. Journal of Phycology.

Wilson, A. E., Sarnelle, O., & Tillmanns, A. R. (2006). Effects of cyanobacterial toxicity and morphology on the population growth of freshwater zooplankton: Meta-analyses of laboratory experiments. Limnology and Oceanography, 51(4), 1915-1924. https://doi.org/10.4319/lo.2006.51.4.1915

Yacobi, Y. Z., Gitelson, A., & Mayo, M. (1995). Remote sensing of chlorophyll in Lake Kinneret using highspectral-resolution radiometer and landsat TM: Spectral features of reflectance and algorithm development. Journal of Plankton Research, 17(11), 2155–2173. https://doi.org/10.1093/plankt/17.11.2155

6. Webography

Agência Portuguesa do Ambiente. https://cnpgb.apambiente.pt/gr_barragens/gbportugal/FICHAS/Aguieiraficha.htm . Last accessed on 28th September 2020.

Agência Portuguesa do Ambiente. https://cnpgb.apambiente.pt/gr_barragens/gbportugal/FICHAS/Alquevaficha.htm . Last accessed on 28th September 2020.

CORINE Land Cover 2018. https://land.copernicus.eu/pan-european/corine-land-cover/clc2018 . Last accessed on 28th September 2020

EC FP7 eartH2Observe project. http://www.earth2observe.eu . Last accessed on 28th September 2020

ESA Diversity II project. http://www.diversity2.info . Last accessed on 28th September 2020

ESA. https://earth.esa.int/web/sentinel/technical-guides/sentinel-2-msi/msi-instrument . Last accessed on 28th September 2020

ESA. https://evdc.esa.int/orbit/ . Last accessed on 28th September 2020

ESA. https://sentinel.esa.int/web/sentinel/missions/sentinel-2 . Last accessed on 28th September 2020

ESA. https://sentinel.esa.int/web/sentinel/missions/sentinel-2/satellite-description . Last accessed on 28th September 2020

USGS. https://www.usgs.gov/earthexplorer-0 . Last accessed on 28th September 2020

7. Appendix I – Histograms of data distribution for Aguieira and Alqueva reservoirs

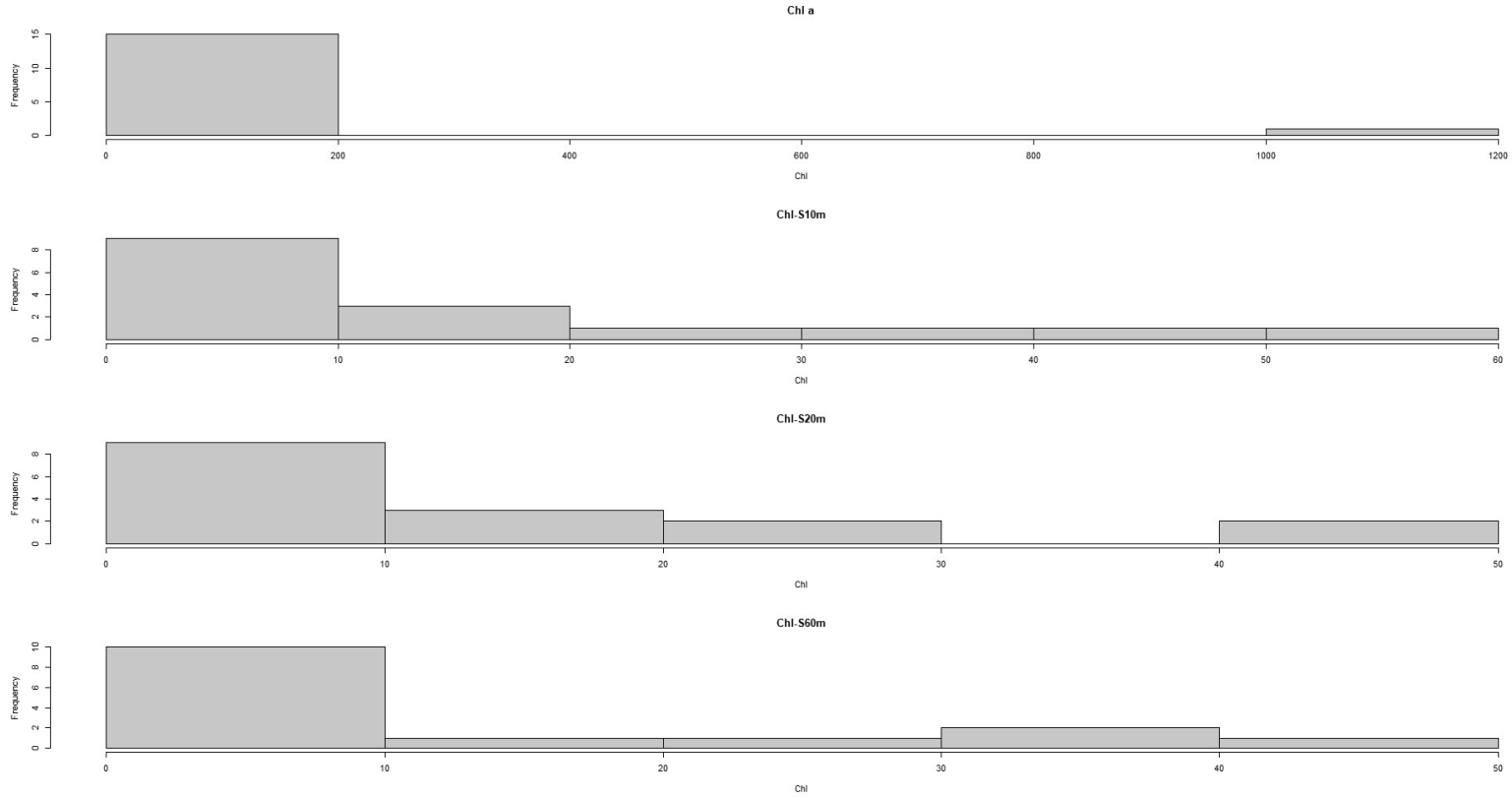

Fig. 10 - Histograms of data distribution of *in situ* measured and satellite estimated [Chl *a*], in Aguieira reservoir.

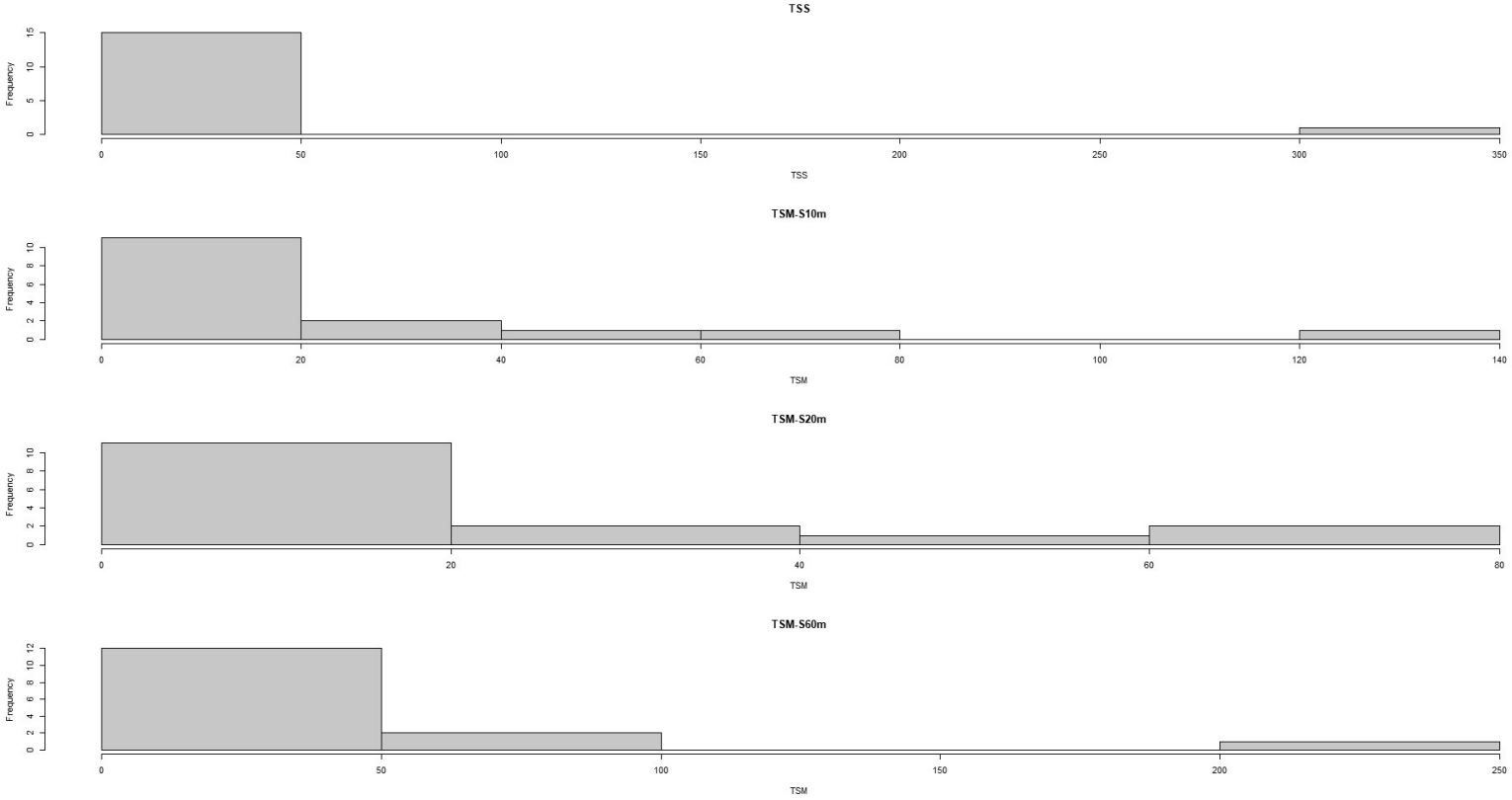

Fig. 11 - Histograms of data distribution of *in situ* measured and satellite estimated [TSS/TSM], in Aguieira reservoir.

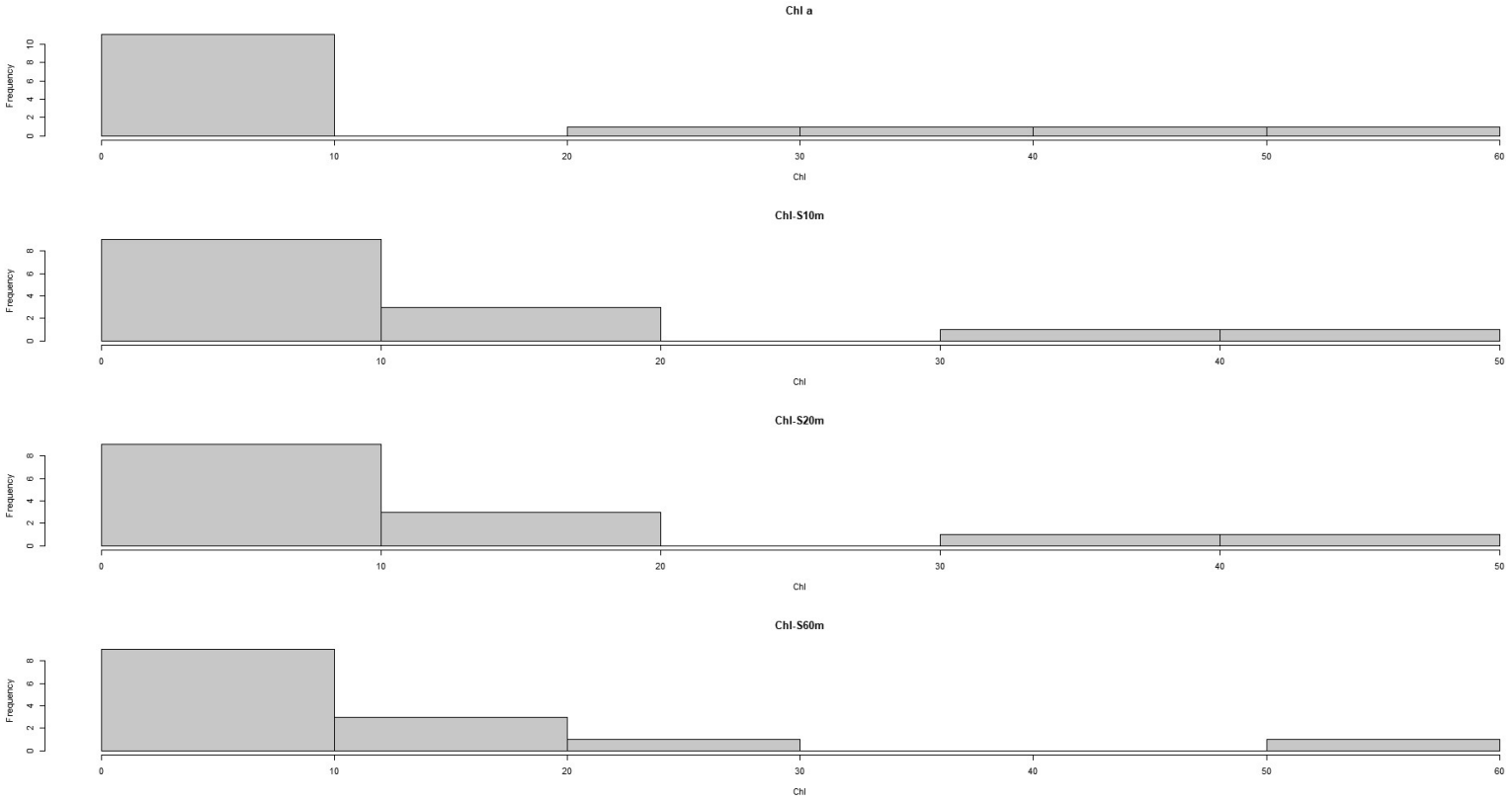

Fig. 12 - Histograms of data distribution of *in situ* measured and satellite estimated [Chl a], in Alqueva reservoir.

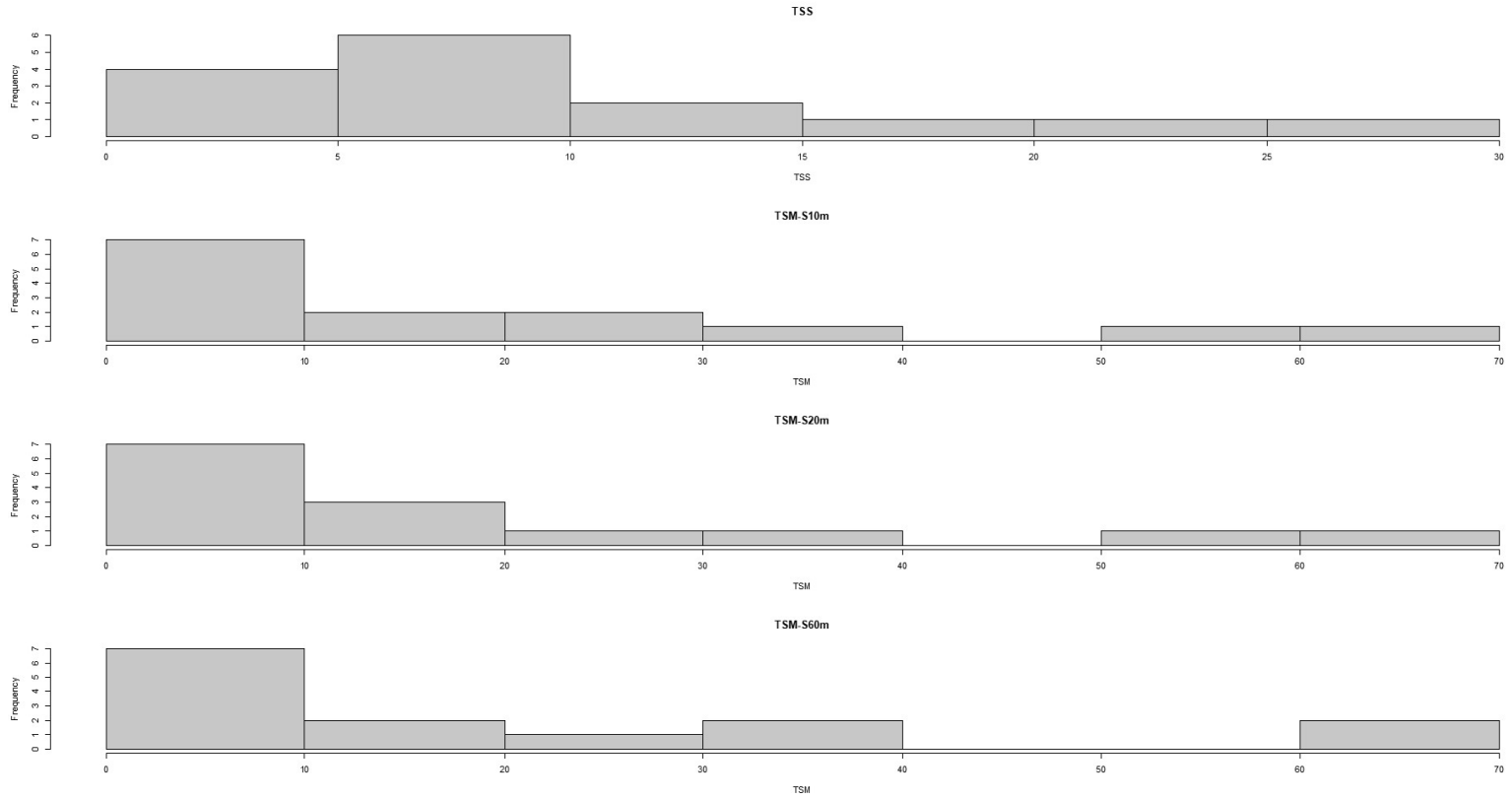

Fig. 13 - Histograms of data distribution of *in situ* measured and satellite estimated [TSS/TSM], in Alqueva reservoir.

8. Appendix II - Datasets used in Principal Component Analysis

Table 8 - Dataset used for Principal Component Analysis for Aguieira reservoir.

site_id	pH	Cond	O_2	Temp	BOD_5	TSS	TSM-10m	TSM-20m	TSM-60m	VSS	Chl *a*
Aut18_A1	8.4	86	8.79	24.5	0.81	8.24	21.456	21.63	6.869	4.17	5.429
Aut18_A2	7.62	96.6	7.97	23.2	0.77	10.09	0.166	0.138	7.551	6.02	10.096
Aut18_A3	8.1	143.2	9.89	21	3.88	312.5	70.421	77.763	83.318	62.5	1082.232
Aut18_A4	7.4	87.4	7.36	24.5	0.48	10.75	6.329	10.129	0.303	7.42	3.438
Spr19_A1	9.2	83.1	11.9	14.4	0.55	13.45	10.922	10.154	19.06	11.07	26.317
Spr19_A2	8.99	89.2	12.4	15	0.86	19.05	0.091	0.145	8.201	14.6	30.62
Spr19_A3	8.31	112	11.3	15.2	0.42	11.08	31.514	26.155	0.5	9.08	10.165
Spr19_A4	9.15	78.2	12.2	15.5	1.12	17.5	0.815	0.763	207.936	13.5	27.904
Aut19_A1	6.83	90.9	4.48	17.7	0.87	7.82	1.889	1.244	2.922	6.75	1.61
Aut19_A2	6.68	92.1	5.29	17.9	1.27	10.75	0.05	0.045	0.167	8.58	2.59
Aut19_A3	6.74	100.9	8.95	16.3	1.56	12.58	124.712	70.101	49.608	7.22	10.96
Aut19_A4	6.8	8.81	6.9	17.3	2.05	5.55	0.035	0.035	NA	4.42	5.3
Spr20_A1	9.608	74.3	12.92	21.9	0.55	15.194	0.219	0.237	0.393	10.806	26.155
Spr20_A2	9.7	85.2	14.18	20.5	0.86	17.542	1.012	0.973	0.306	10.958	42.078
Spr20_A3	8.999	89.6	12.39	20.7	0.42	16.625	44.223	43.835	26.28	11.542	19.033

site_id	pH	Cond	O_2	Temp	BOD_5	TSS	TSM-10m	TSM-20m	TSM-60m	VSS	Chl *a*
Spr20_A4	9.4	72.8	13.28	22.4	1.12	11.233	0.221	0.255	82.503	6.633	31.752
site_id	**Chl-S10m**	**Chl-S20m**	**Chl-S60m**	**Turb**	**DOC**	**TH**	**Fe**	**Mn**	**As**	**Cd**	**Cu**
Aut18_A1	15.979	13.524	6.64	0.018	0.059	22.1	36	3.26	1.77	0.07	0.74
Aut18_A2	0.08	0.021	9.973	0.036	0.082	1.7	220	14.2	2.13	0.02	2.87
Aut18_A3	33.615	42.538	41.227	0.115	0.151	1.8	360	65.7	2.95	0.06	2.19
Aut18_A4	15.236	21.456	3.691	0.038	0.043	1.8	190	29.2	3.34	0.01	2.42
Spr19_A1	1.266	3.31	9.42	0.072	0.1	1.6	45	4.34	0.93	0.02	2.37
Spr19_A2	0.177	0.101	2.703	0.069	0.23	1.7	57	4.78	0.93	0.01	0.98
Spr19_A3	22.05	14.531	1.84	0.087	0.148	1.9	110	12.8	1.48	0.01	0.99
Spr19_A4	11.996	11.158	32.3	0.074	0.243	1.6	71	6.04	2.2	0.03	0.85
Aut19_A1	0.931	1.336	1.278	0.023	0.014	1.8	170	44.8	1.45	9.00E-18	1.51
Aut19_A2	0.198	0.319	0.626	0.035	0.037	1.8	220	25.7	1.6	0.01	1.11
Aut19_A3	57.304	22.514	33.832	0.046	0.048	2	260	24.8	1.77	0.02	1.68
Aut19_A4	0.301	0.299		0.016	0.03	1.7	120	19.3	1.69	9.00E-18	1.08
Spr20_A1	1.152	1.096	1.443	8.00E-03	0.056	1.4	180	4.74	1.41	0.02	1.86
Spr20_A2	2.114	1.726	9.55E-04	8.00E-03	0.072	1.5	190	6.1	1.31	0.02	2.09
Spr20_A3	45.97	47.207	29.177	0.015	0.033	1.7	250	8.79	1.62	0.02	2.92
Spr20_A4	0.592	0.658	19.872	8.00E-03	0.046	1.3	190	7.77	2.83	0.01	1.7

site_id	Hg	Ni	Pb	Zn	COD	NH_4	N	NO_3	NO_2	P
Aut18_A1	9.00E-18	9.00E-18	1	1.4	10	9.00E-18	0	1.3	9.00E-18	9.00E-18
Aut18_A2	0.04	1.1	1	16	18	9.00E-18	9.00E-18	9.00E-18	0.02	0.03
Aut18_A3	0.02	0.9	0.7	14.2	90	9.00E-18	6.3	9.00E-18	9.00E-18	0.22
Aut18_A4	0.02	0.8	0.4	11	9.00E-18	9.00E-18	9.00E-18	2.4	0.01	0.03
Spr19_A1	0.02	0.6	0.5	6.7	53	0.07	9.00E-18	2.8	0.04	0.01
Spr19_A2	0.02	0.6	0.2	12.8	51	9.00E-18	9.00E-18	3.3	0.07	0.01
Spr19_A3	0.02	0.4	0.2	6.7	45	0.06	9.00E-18	4	0.04	0.09
Spr19_A4	0.02	0.3	0.6	6.8	50	0.09	0.7	1.2	0.02	0.02
Aut19_A1	0.18	0.6	0.2	7.3	33	9.00E-18	9.00E-18	1.5	9.00E-18	9.00E-18
Aut19_A2	0.14	0.5	0.2	9.4	36	9.00E-18	9.00E-18	1.2	9.00E-18	9.00E-18
Aut19_A3	0.13	0.6	0.6	10.8	49	9.00E-18	2.2	2.3	0.02	0.09
Aut19_A4	0.11	0.7	0.4	20.3	29	9.00E-18	0.6	1	0.03	9.00E-18
Spr20_A1	1.85	2.3	0.4	32.2	44	0.07	9.00E-18	2.7	0.04	0.02
Spr20_A2	1.57	1.7	0.3	27.7	48	0.07	0.7	2.2	0.04	0.03
Spr20_A3	1.33	1.6	0.4	28.9	43	0.18	9.00E-18	3.3	0.05	0.08
Spr20_A4	0.63	1.5	0.3	24.7	47	0.1	9.00E-18	0.6	0.01	0.03

Table 9 - Dataset used for Principal Component Analysis for Alqueva reservoir.

site_id	pH	Cond	O_2	Temp	BOD_5	TSS	TSM-S10m	TSM-S20m	TSM-S60m	VSS	Chl *a*
Aut18_Al1	7.931	501.000	6.580	16.600	0.560	4.280	65.274	56.571	62.241	2.280	0.980
Aut18_Al2	8.019	491.000	7.440	17.200	0.450	3.830	17.211	16.738	39.680	2.280	3.596
Aut18_Al3	8.124	515.000	6.990	16.800	0.740	4.720	35.153	35.132	31.673	4.060	1.812
Aut18_Al4	8.047	541.000	6.580	17.600	1.070	3.610	1.590	1.835	1.836	2.060	2.183
Aut18_Al5	8.389	692.000	11.550	16.600	4.350	15.420	11.742	10.515	13.666	10.080	31.257
Spr19_Al1	8.544	517.000	9.640	23.000	0.560	7.750	NA	NA	NA	6.080	2.285
Spr19_Al2	8.710	515.000	9.390	23.700	2.250	7.420	5.789	8.839	1.683	6.420	0.936
Spr19_Al3	8.790	538.000	9.990	23.100	0.840	7.420	3.780	3.780	17.354	5.750	2.494
Spr19_Al4	8.540	570.000	12.720	23.800	1.730	12.750	0.429	0.412	0.412	9.420	7.832
Spr19_Al5	9.050	714.000	16.930	23.000	11.385	20.420	0.798	0.620	9.208	14.080	56.649
Aut19_Al1	8.233	525.000	8.050	16.600	1.930	10.020	NA	NA	NA	8.620	3.534
Aut19_Al2	8.331	521.000	8.040	16.900	1.330	24.720	NA	NA	NA	21.720	8.276
Aut19_Al3	8.322	545.000	8.540	16.900	1.280	7.880	NA	NA	NA	6.380	2.747
Aut19_Al4	8.260	578.000	7.510	16.900	1.240	8.780	NA	NA	NA	7.050	2.806
Aut19_Al5	8.376	769.000	10.960	14.600	3.850	29.970	NA	NA	NA	23.370	40.103
Spr20_Al1	8.780	540.000	8.290	32.000	0.730	6.250	57.902	64.258	68.173	5.817	2.197

site_id	pH	Cond	O_2	Temp	BOD_5	TSS	TSM-S10m	TSM-S20m	TSM-S60m	VSS	Chl *a*
Spr20_Al2	8.870	506.000	8.480	33.300	0.700	7.083	21.194	21.105	21.541	5.917	2.281
Spr20_Al3	8.960	558.000	8.430	31.700	1.470	6.317	8.154	8.155	8.506	4.617	3.675
Spr20_Al4	9.210	509.000	10.010	32.000	1.810	10.021	7.601	7.473	7.467	5.562	20.777
Spr20_Al5	8.590	588.000	7.040	32.000	4.360	28.500	21.375	15.846	1.538	23.833	45.419
site_id	**Chl-S10m**	**Chl-S20m**	**Chl-S60m**	**Turb**	**DOC**	**TH**	**Fe**	**Mn**	**As**	**Cd**	**Cu**
Aut18_Al1	11.446	12.720	16.028	2.300E-03	0.0736	13.700	46.000	13.000	2.980	0.030	1.510
Aut18_Al2	1.748	1.717	14.630	0	0.138	16.200	7.000	6.540	2.350	9.000E-18	0.620
Aut18_Al3	12.824	12.832	10.780	0.023	0.067	16.700	15.000	10.900	3.540	9.000E-18	0.520
Aut18_Al4	3.830E-04	3.760E-04	3.760E-04	0.014	0.090	17.500	23.000	9.500	4.850	9.000E-18	0.520
Aut18_Al5	5.492E-03	8.710E-04	1.975	0.044	0.248	23.100	140.000	28.700	2.370	0.020	1.730
Spr19_Al1	NA	NA	NA	9.200E-03	0.3795	16.400	9.000	4.330	1.750	9.000E-18	4.360
Spr19_Al2	1.818	0.105	3.473E-03	0.012	0.384	16.500	12.000	3.860	1.600	9.000E-18	3.490
Spr19_Al3	0.436	0.436	4.169	2.300E-03	0.3864	17.300	15.000	4.890	1.750	9.000E-18	3.890
Spr19_Al4	3.730E-04	3.660E-04	3.660E-04	0.016	0.352	18.300	18.000	10.900	2.180	9.000E-18	3.240
Spr19_Al5	0.858	0.585	2.567	0.074	0.460	19.900	85.000	55.300	4.910	9.000E-18	3.390
Aut19_Al1	NA	NA	NA	0.023	0.041	17.400	44.000	54.700	4.310	9.000E-18	0.720
Aut19_Al2	NA	NA	NA	0.021	0.053	17.800	200.000	52.000	3.690	9.000E-18	1.120
Aut19_Al3	NA	NA	NA	0.018	0.044	17.900	67.000	21.200	3.710	9.000E-18	0.600

site_id	Chl-S10m	Chl-S20m	Chl-S60m	Turb	DOC	TH	Fe	Mn	As	Cd	Cu
Aut19_Al4	NA	NA	NA	0.021	0.067	18.100	93.000	33.300	4.780	9.000E-18	0.950
Aut19_Al5	NA	NA	NA	0.092	0.087	26.400	280.000	97.300	3.080	0.010	1.110
Spr20_Al1	47.183	44.599	53.677	7.700E-03	0.056	18.500	210.000	9.580	2.020	0.050	1.800
Spr20_Al2	12.530	13.498	22.423	2.600E-03	0.056	18.300	190.000	7.100	2.300	0.020	2.260
Spr20_Al3	7.150E-04	7.260E-04	4.530E-04	7.700E-03	0.069	19.100	200.000	6.000	2.700	0.020	2.210
Spr20_Al4	1.107	0.355	0.361	0.038	0.115	18.400	210.000	12.900	4.420	0.020	2.370
Spr20_Al5	38.058	31.452	1.217	0.082	0.153	19.600	570.000	79.200	7.780	0.020	2.660

site_id	Hg	Ni	Pb	Zn	COD	NH_4	N	NO_3	NO_2	P
Aut18_Al1	0.020	0.600	0.300	5.200	9.000	9.000E-18	9.000E-18	4.500	9.000E-18	0.060
Aut18_Al2	9.000E-18	0.500	0.100	2.700	16.000	9.000E-18	9.000E-18	0.500	0.020	0.030
Aut18_Al3	9.000E-18	0.600	9.000E-18	7.100	12.000	0.170	9.000E-18	9.000E-18	0.120	0.070
Aut18_Al4	9.000E-18	0.700	9.000E-18	6.500	18.000	0.200	9.000E-18	0.800	0.520	0.080
Aut18_Al5	9.000E-18	1.200	0.500	9.600	17.000	9.000E-18	1.300	5.600	0.080	0.160
Spr19_Al1	9.000E-18	0.600	9.000E-18	2.700	59.000	0.050	0.600	9.000E-18	0.010	0.010
Spr19_Al2	9.000E-18	0.500	9.000E-18	1.000	51.000	9.000E-18	0.600	9.000E-18	0.020	9.000E-18
Spr19_Al3	9.000E-18	0.600	0.100	4.100	53.000	0.110	0.600	0.600	0.040	0.010
Spr19_Al4	0.140	0.600	0.100	1.200	54.000	0.080	0.700	0.700	0.070	0.010
Spr19_Al5	9.000E-18	1.100	0.500	3.200	60.000	0.580	2.100	0.900	1.700	0.090

site_id	Hg	Ni	Pb	Zn	COD	NH_4	N	NO_3	NO_2	P
Aut19_AI1	0.040	0.800	9.000E-18	6.100	44.000	9.000E-18	9.000E-18	9.000E-18	0.020	0.070
Aut19_AI2	0.020	0.900	0.200	5.900	44.000	9.000E-18	0.500	9.000E-18	0.040	0.050
Aut19_AI3	0.040	0.600	0.100	5.400	43.000	0.190	0.700	9.000E-18	0.040	0.040
Aut19_AI4	0.060	0.900	0.200	8.300	52.000	0.280	1.000	0.500	0.660	0.050
Aut19_AI5	0.020	1.600	0.700	6.300	44.000	0.810	1.600	1.700	0.120	0.070
Spr20_AI1	4.780	3.200	2.100	691.000	40.000	9.000E-18	9.000E-18	9.000E-18	0.020	0.040
Spr20_AI2	2.200	2.400	0.500	89.200	46.000	9.000E-18	9.000E-18	9.000E-18	0.020	0.050
Spr20_AI3	2.370	2.700	0.400	51.300	50.000	9.000E-18	0.600	0.800	0.090	0.030
Spr20_AI4	2.370	2.900	0.400	41.200	55.000	9.000E-18	0.800	9.000E-18	0.090	0.060
Spr20_AI5	2.040	3.300	1.000	51.400	56.000	0.160	1.000	9.000E-18	0.040	0.180

Table 10 - Dataset used for Principal Component Analysis for Aguieira and Alqueva reservoirs.

site_id	reservoir	Chl *a*	Chl-S10m	Chl-S20m	Chl-S60m	TSS	TSM-S10m	TSM-S20m	TSM-S60m
Aut18_A1	**Aguieira**	5.429	15.979	13.524	6.640	8.240	21.456	21.630	6.869
Aut18_A2	**Aguieira**	10.096	0.080	0.021	9.973	10.090	0.166	0.138	7.551
Aut18_A3	**Aguieira**	1082.232	33.615	42.538	41.227	312.500	70.421	77.763	83.318
Aut18_A4	**Aguieira**	3.438	15.236	21.456	3.691	10.750	6.329	10.129	0.303
Spr19_A1	**Aguieira**	26.317	1.266	3.310	9.420	13.450	10.922	10.154	19.060
Spr19_A2	**Aguieira**	30.620	0.177	0.101	2.703	19.050	0.091	0.145	8.201
Spr19_A3	**Aguieira**	10.165	22.050	14.531	1.840	11.080	31.514	26.155	0.500
Spr19_A4	**Aguieira**	27.904	11.996	11.158	32.300	17.500	0.815	0.763	207.936
Aut19_A1	**Aguieira**	1.610	0.931	1.336	1.278	7.820	1.889	1.244	2.922
Aut19_A2	**Aguieira**	2.590	0.198	0.319	0.626	10.750	0.050	0.045	0.167
Aut19_A3	**Aguieira**	10.960	57.304	22.514	33.832	12.580	124.712	70.101	49.608
Aut19_A4	**Aguieira**	5.300	0.301	0.299	NA	5.550	0.035	0.035	NA
Spr20_A1	**Aguieira**	26.155	1.152	1.096	1.443	15.194	0.219	0.237	0.393
Spr20_A2	**Aguieira**	42.078	2.114	1.726	9.55E-04	17.542	1.012	0.973	0.306
Spr20_A3	**Aguieira**	19.033	45.970	47.207	29.177	16.625	44.223	43.835	26.280
Spr20_A4	**Aguieira**	31.752	0.592	0.658	19.872	11.233	0.221	0.255	82.503
Aut18_Al1	**Alqueva**	0.980	11.446	12.720	16.028	4.280	65.274	56.571	62.241

site_id	reservoir	Chl *a*	Chl-S10m	Chl-S20m	Chl-S60m	TSS	TSM-S10m	TSM-S20m	TSM-S60m
Aut18_Al2	**Alqueva**	3.596	1.748	1.717	14.630	3.830	17.211	16.738	39.680
Aut18_Al3	**Alqueva**	1.812	12.824	12.832	10.780	4.720	35.153	35.132	31.673
Aut18_Al4	**Alqueva**	2.183	3.83E-04	3.76E-04	3.76E-04	3.610	1.590	1.835	1.836
Aut18_Al5	**Alqueva**	31.257	5.49E-03	8.71E-04	1.975	15.420	11.742	10.515	13.666
Spr19_Al1	**Alqueva**	2.285	NA	NA	NA	7.750	NA	NA	NA
Spr19_Al2	**Alqueva**	0.936	1.818	0.105	0.003	7.420	5.789	8.839	1.683
Spr19_Al3	**Alqueva**	2.494	0.436	0.436	4.169	7.420	3.780	3.780	17.354
Spr19_Al4	**Alqueva**	7.832	3.73E-04	3.66E-04	3.66E-04	12.750	0.429	0.412	0.412
Spr19_Al5	**Alqueva**	56.649	0.858	0.585	2.567	20.420	0.798	0.620	9.208
Aut19_Al1	**Alqueva**	3.534	NA	NA	NA	10.020	NA	NA	NA
Aut19_Al2	**Alqueva**	8.276	NA	NA	NA	24.720	NA	NA	NA
Aut19_Al3	**Alqueva**	2.747	NA	NA	NA	7.880	NA	NA	NA
Aut19_Al4	**Alqueva**	2.806	NA	NA	NA	8.780	NA	NA	NA
Aut19_Al5	**Alqueva**	40.103	NA	NA	NA	29.970	NA	NA	NA
Spr20_Al1	**Alqueva**	2.197	47.183	44.599	53.677	6.250	57.902	64.258	68.173
Spr20_Al2	**Alqueva**	2.281	12.530	13.498	22.423	7.083	21.194	21.105	21.541
site_id	**reservoir**	**Chl *a***	**Chl-S10m**	**Chl-S20m**	**Chl-S60m**	**TSS**	**TSM-S10m**	**TSM-S20m**	**TSM-S60m**
Spr20_Al3	**Alqueva**	3.675	7.15E-04	7.26E-04	4.53E-04	6.317	8.154	8.155	8.506

site_id	reservoir	Chl *a*	Chl-S10m	Chl-S20m	Chl-S60m	TSS	TSM-S10m	TSM-S20m	TSM-S60m
Spr20_Al4	**Alqueva**	20.777	1.107	0.355	0.361	10.021	7.601	7.473	7.467
Spr20_Al5	**Alqueva**	45.419	38.058	31.452	1.217	28.500	21.375	15.846	1.538

9. Appendix III – Reservoir maps concerning the bands “conc_chl” and “conc_tsm”

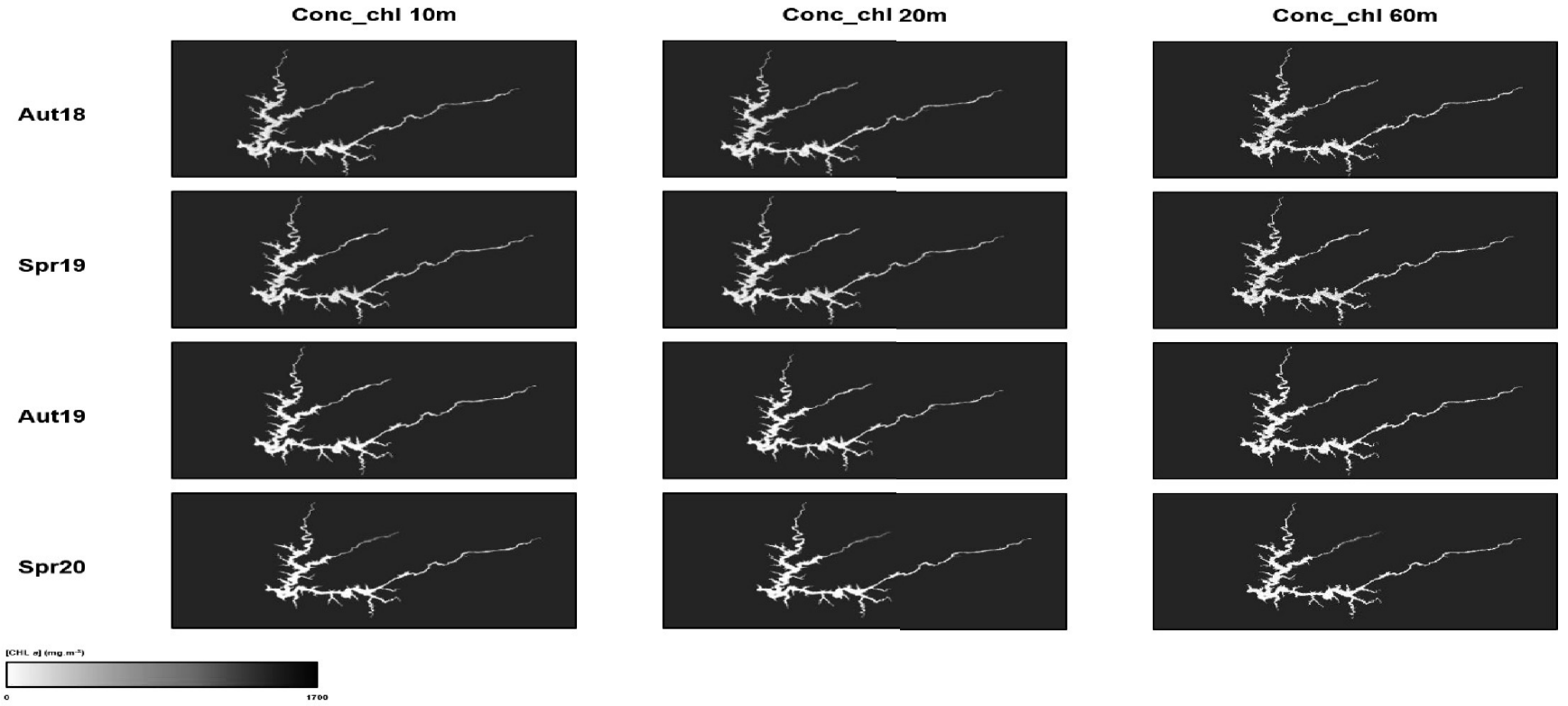

Fig. 14 - Maps of the Aguieira reservoir concerning the band "conc_chl".

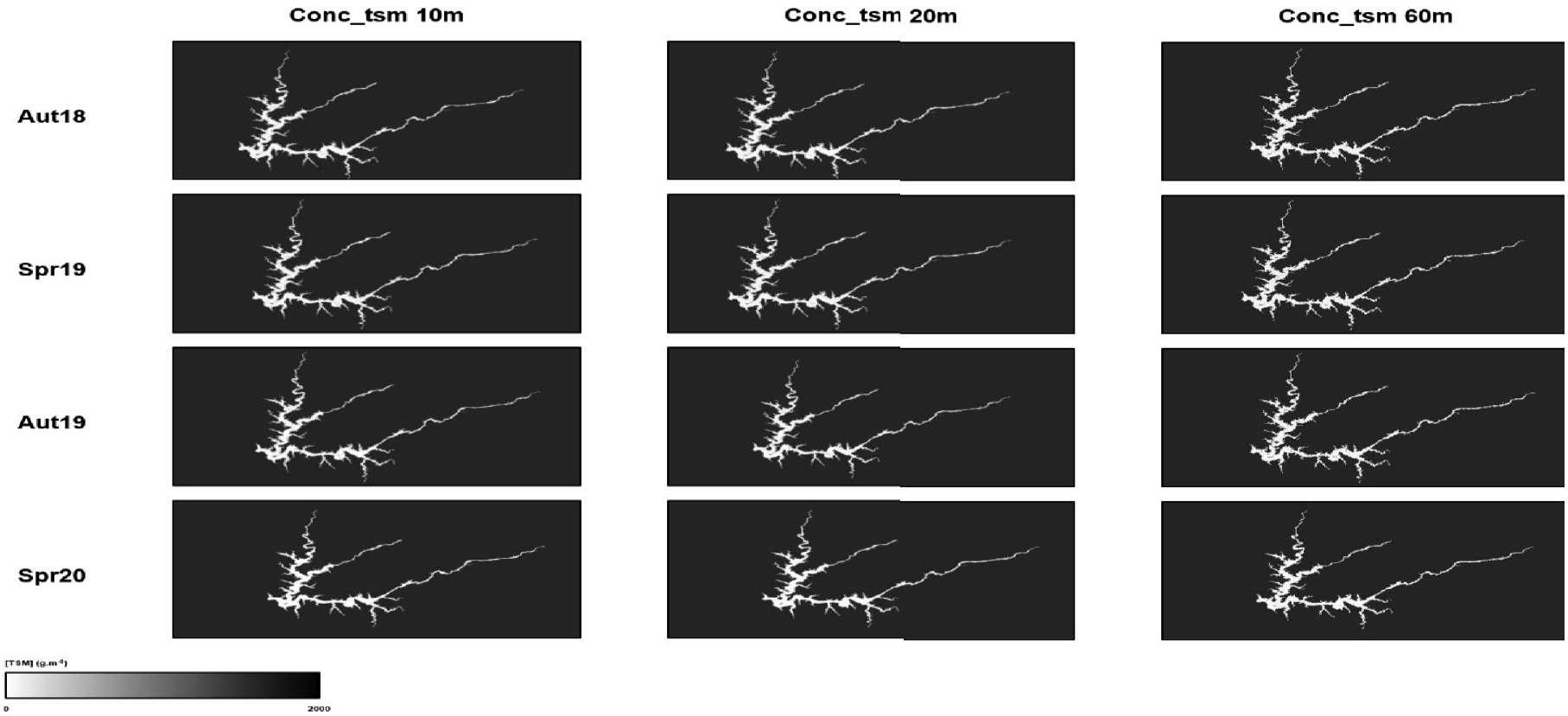

Fig. 15 - Maps of the Aguieira reservoir concerning the band "conc_tsm".

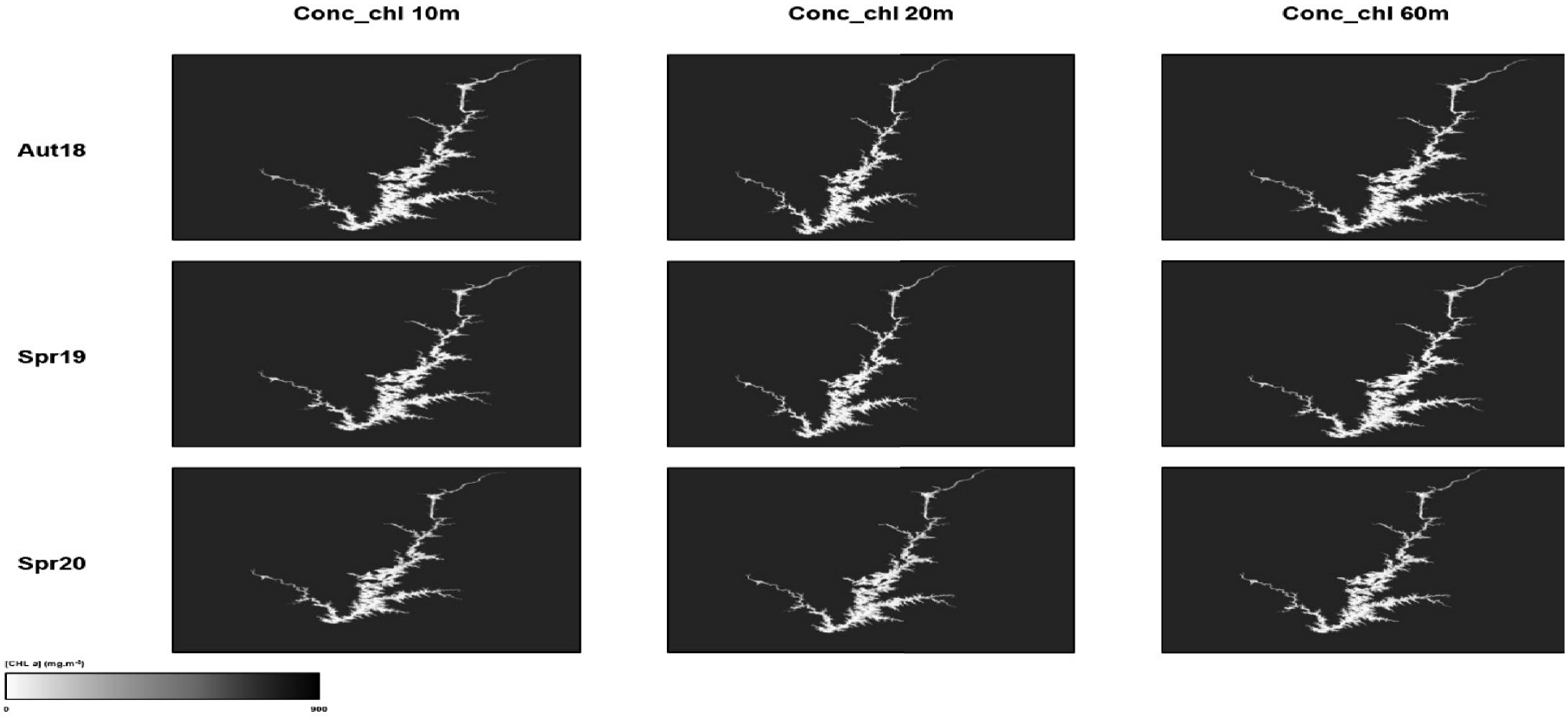

Fig. 16 - Maps of the Alqueva reservoir concerning the band "conc_chl".

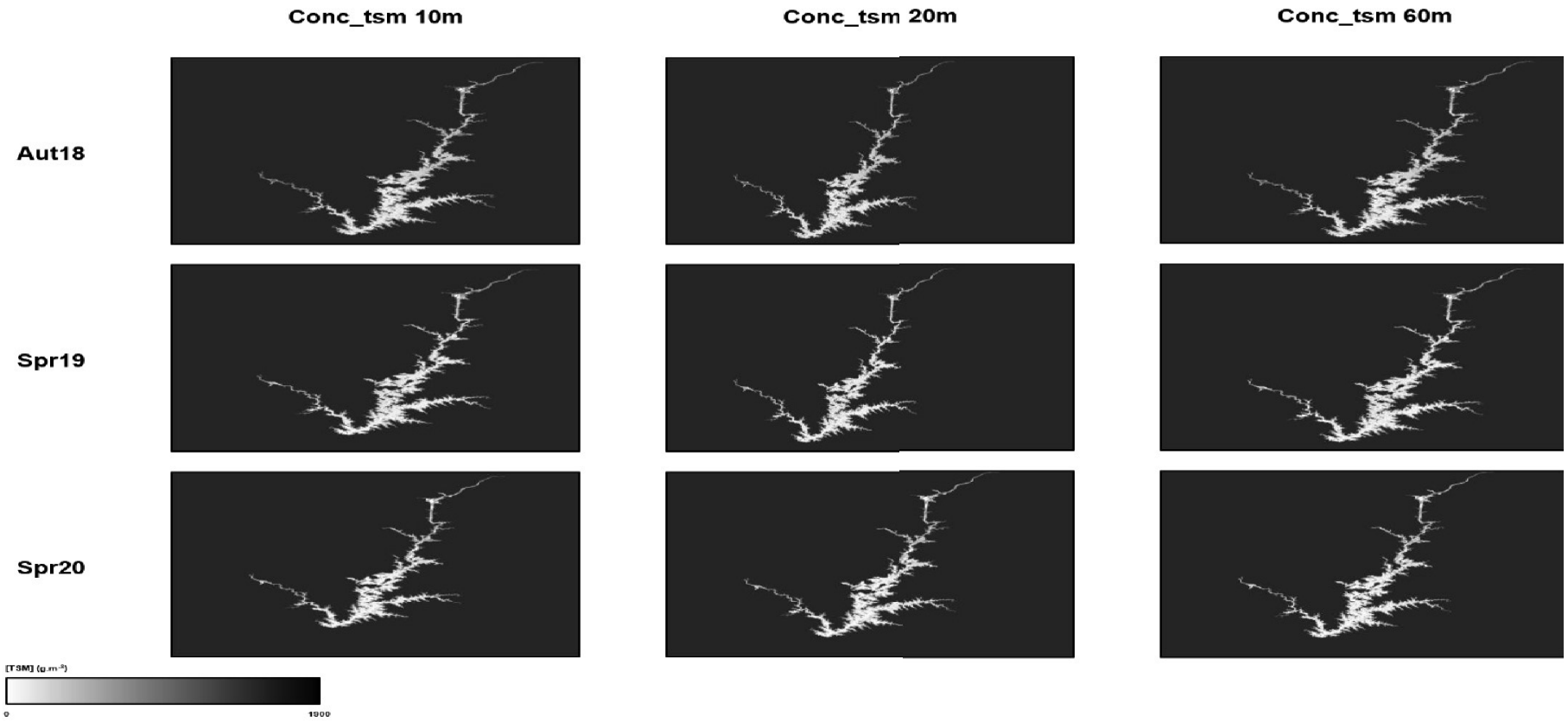

Fig. 17 - Maps of the Alqueva reservoir concerning the band "conc_tsm".

10. Appendix IV – Plots: *In situ* vs SNAP-C2RCC estimates

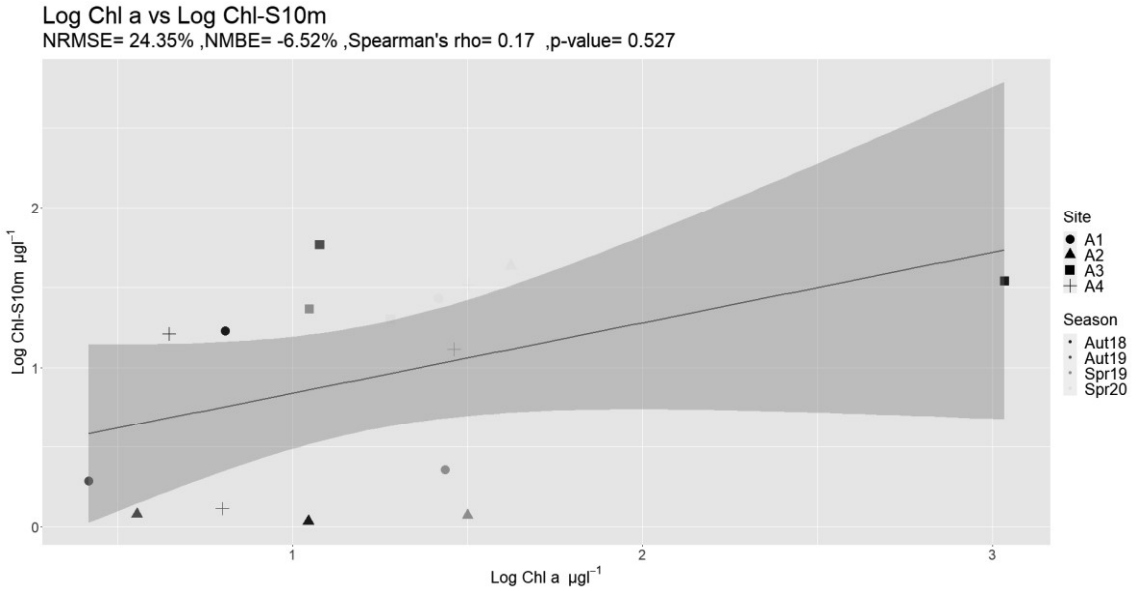

Fig. 18 - Aguieira reservoir; Log [Chl *a*] from Chl-S10m plotted against Log [Chl *a*] measured *in situ*.

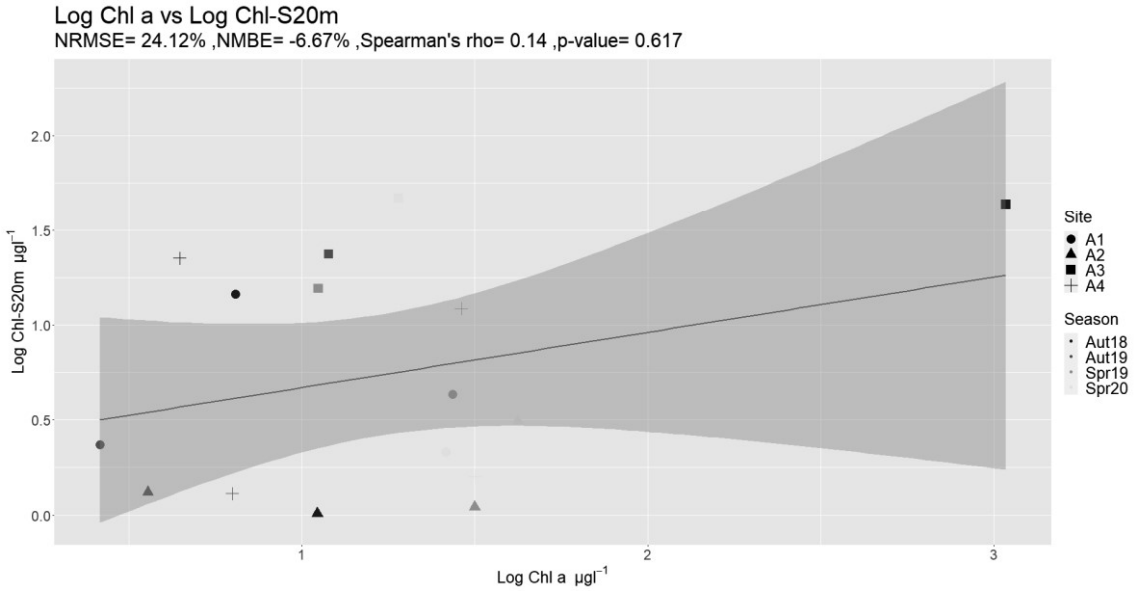

Fig. 19 - Aguieira reservoir; Log [Chl *a*] from Chl-S20m plotted against Log [Chl *a*] measured *in situ*.

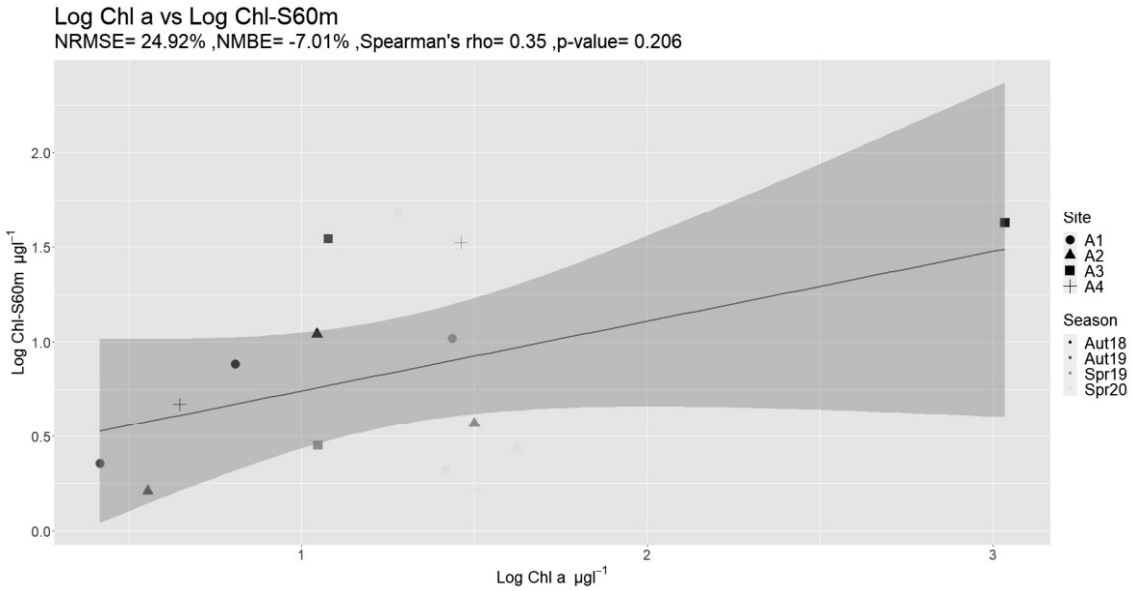

Fig. 20 - Aguieira reservoir; Log [Chl *a*] from Chl-S60m plotted against Log [Chl *a*] measured *in situ*.

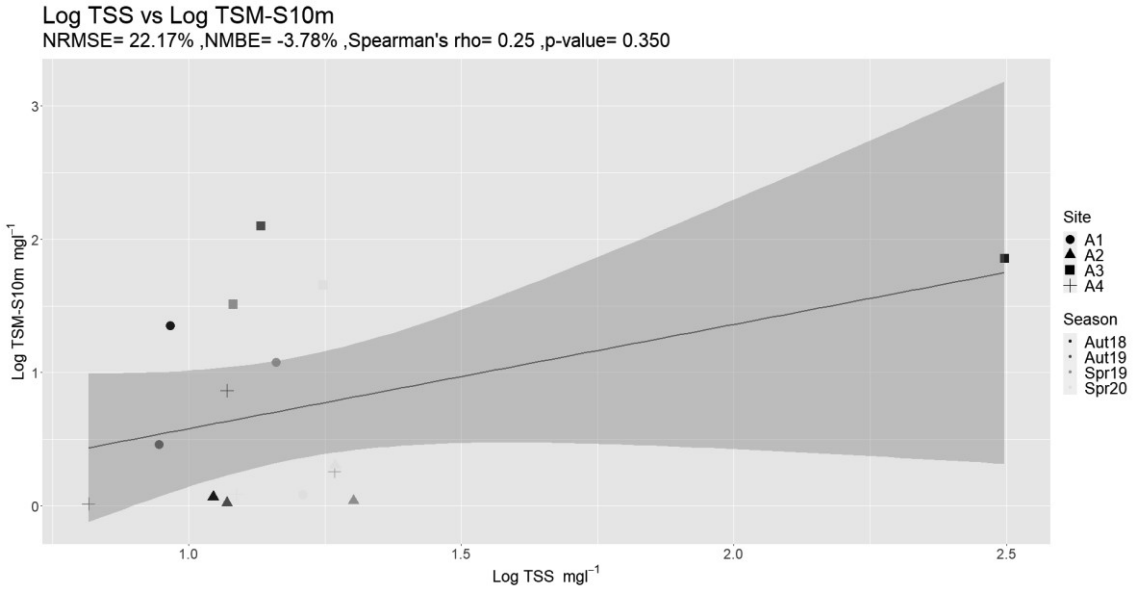

Fig. 21 - Aguieira reservoir; Log [TSM] from TSM-S10m plotted against Log [TSS] measured *in situ*.

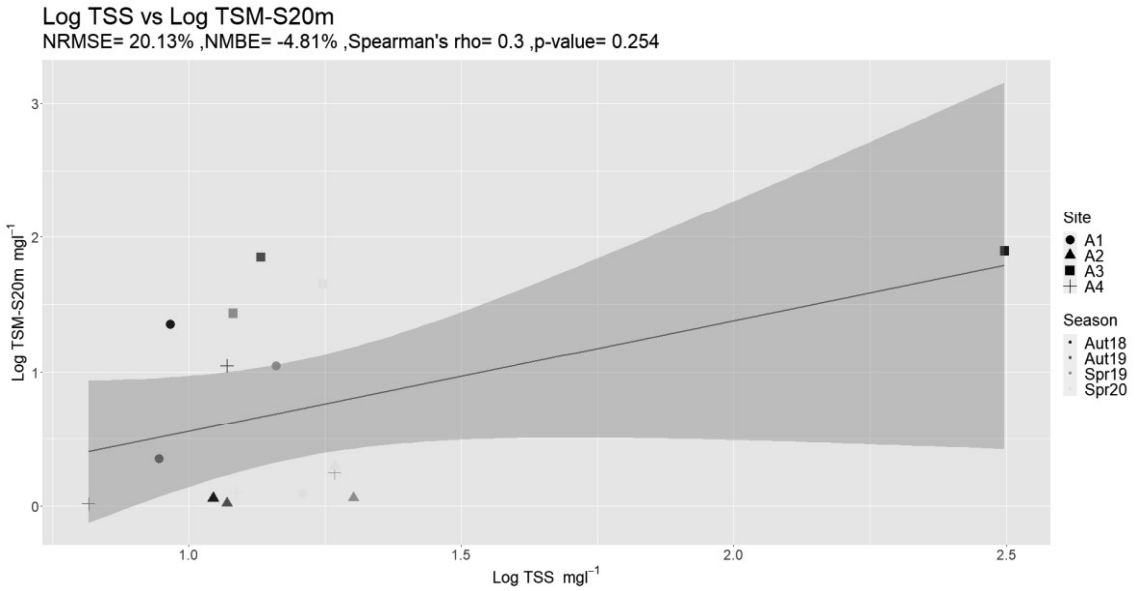

Fig. 22 - Aguieira reservoir; Log [TSM] from TSM-S20m plotted against Log [TSS] measured *in situ*.

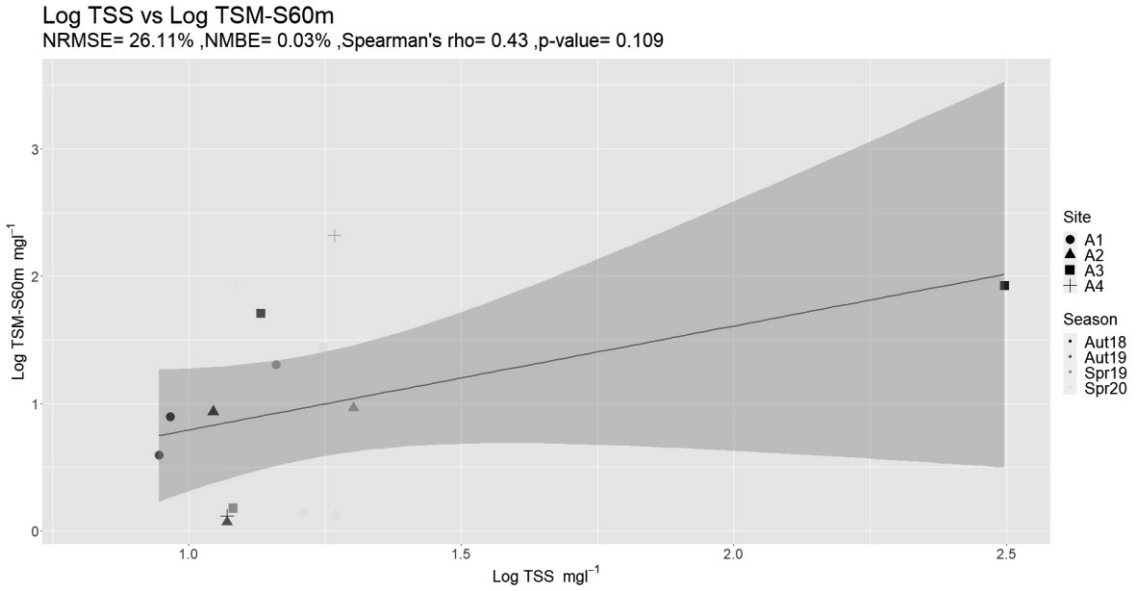

Fig. 23 - Aguieira reservoir; Log [TSM] from TSM-S60m plotted against Log [TSS] measured *in situ*.

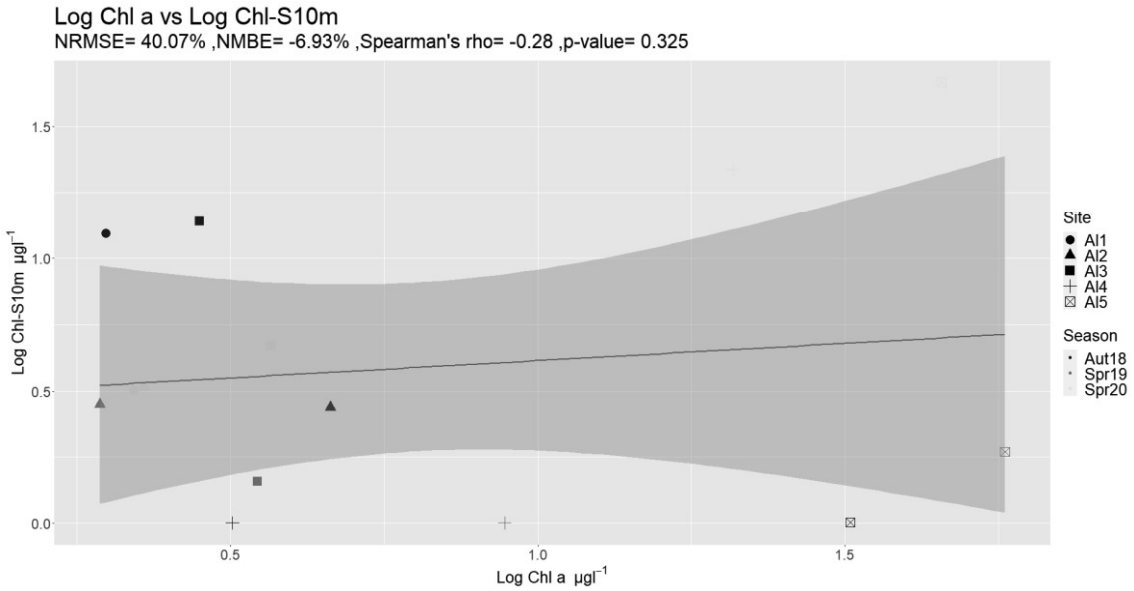

Fig. 24 - Alqueva reservoir; Log [Chl *a*] from Chl-S10m plotted against Log [Chl *a*] measured *in situ*.

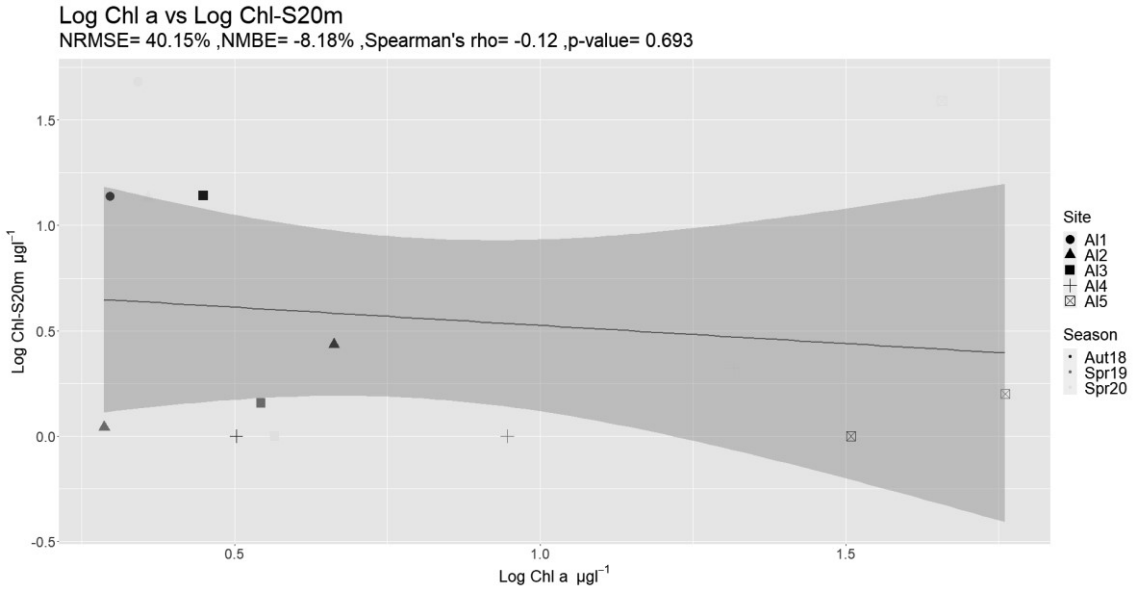

Fig. 25 - Alqueva reservoir; Log [Chl *a*] from Chl-S20m plotted against Log [Chl *a*] measured *in situ*.

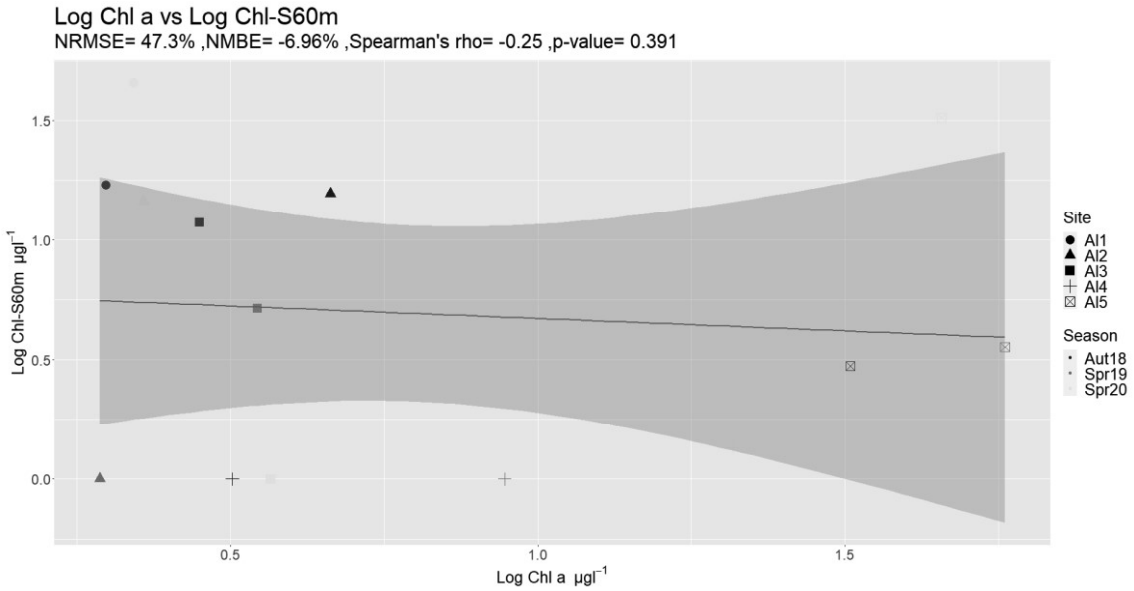

Fig. 26 - Alqueva reservoir; Log [Chl *a*] from Chl-S60m plotted against Log [Chl *a*] measured *in situ*.

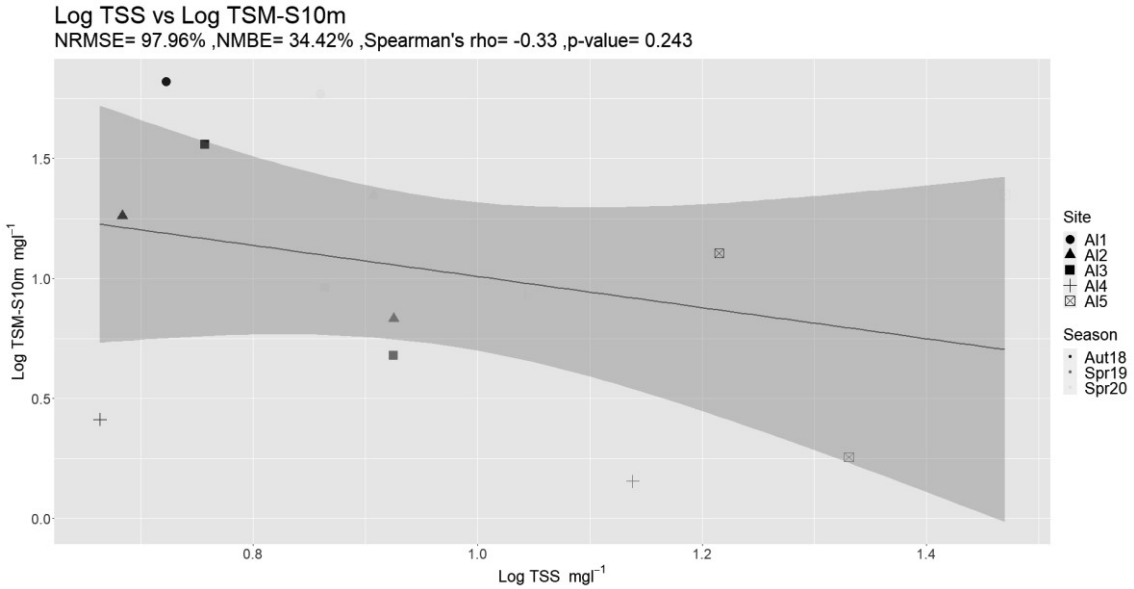

Fig. 27 - Alqueva reservoir; Log [TSM] from TSM-S10m plotted against Log [TSS] measured *in situ*.

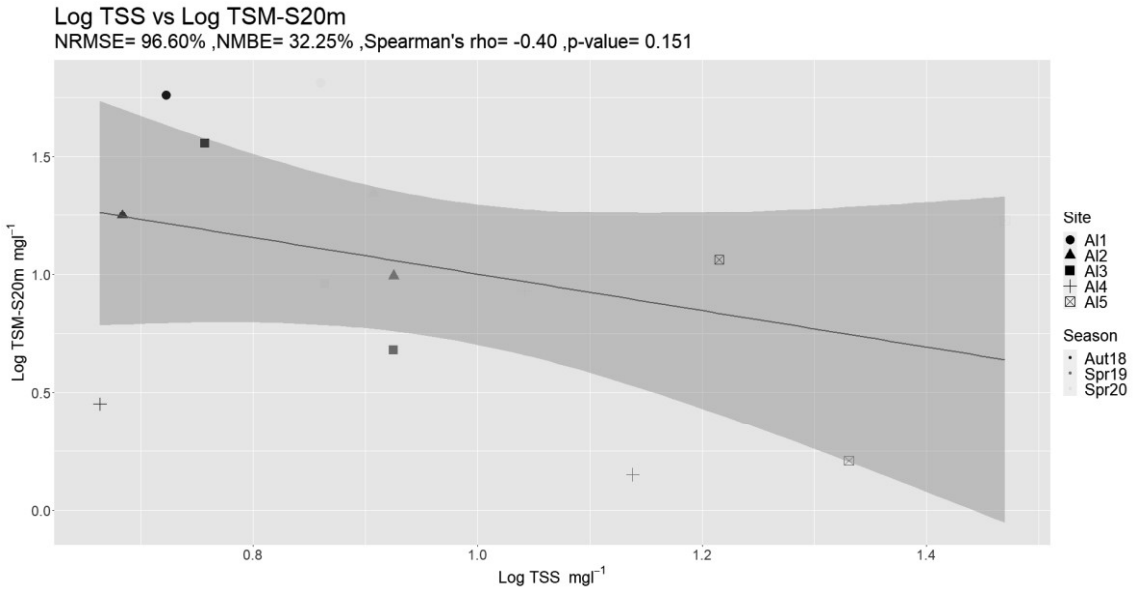

Fig. 28 - Alqueva reservoir; Log [TSM] from TSM-S20m plotted against Log [TSS] measured *in situ*.

11.Appendix V – Loading scores

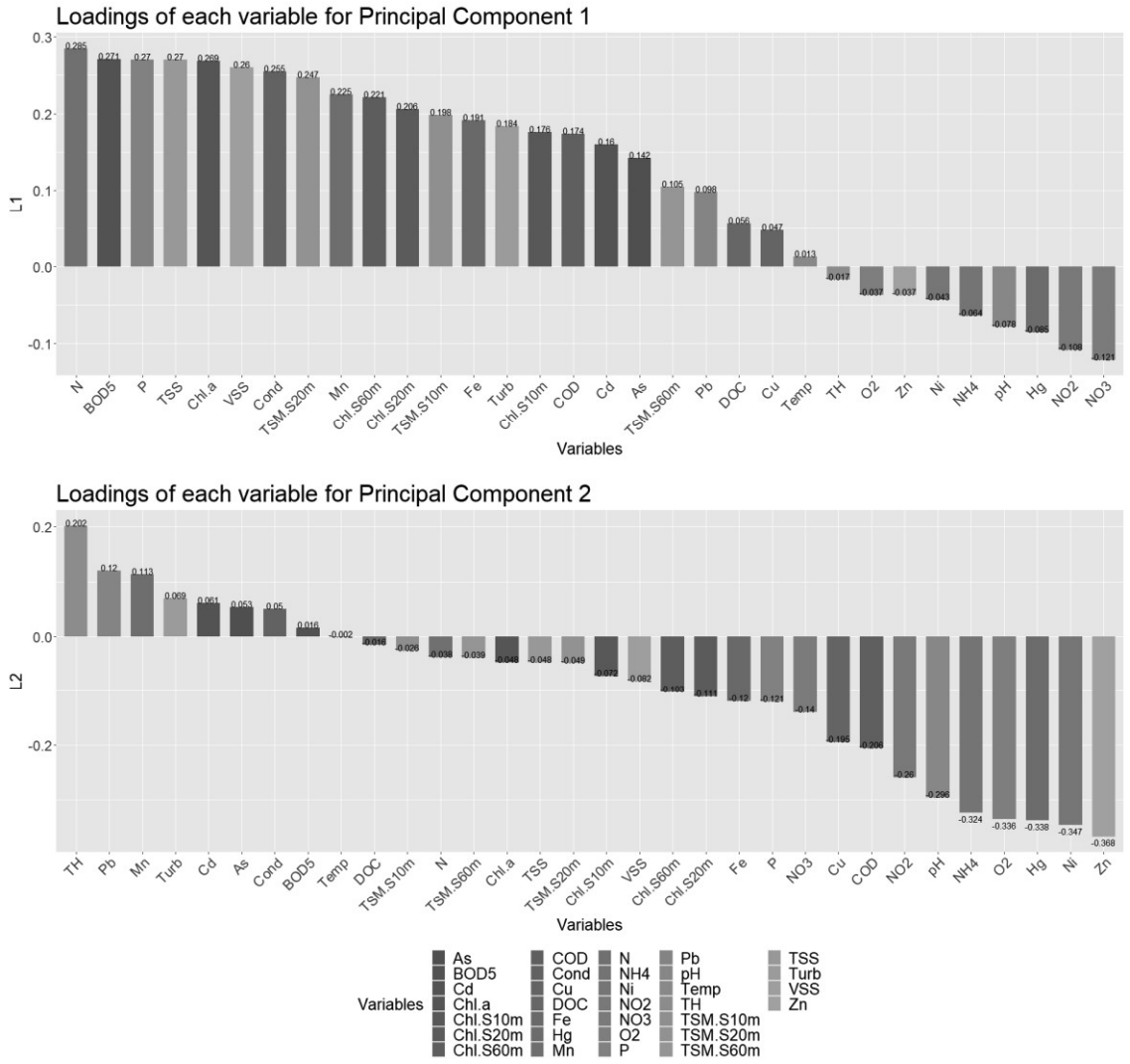

Fig. 29 – Loading scores of Aguieira variables for PC1 (above) and PC2 (below).

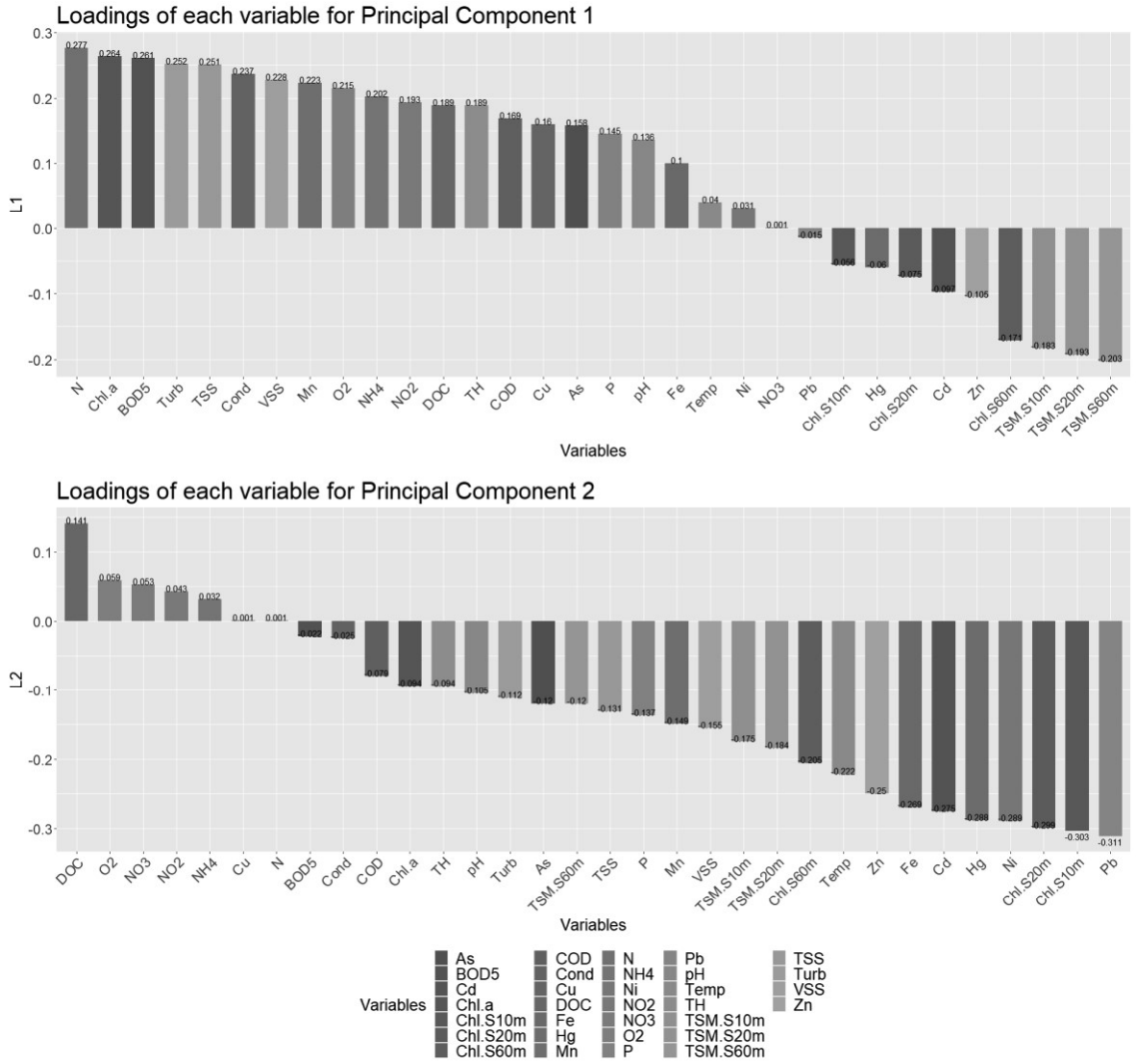

Fig. 30 - Loading scores of Alqueva variables for PC1 (above) and PC2 (below).

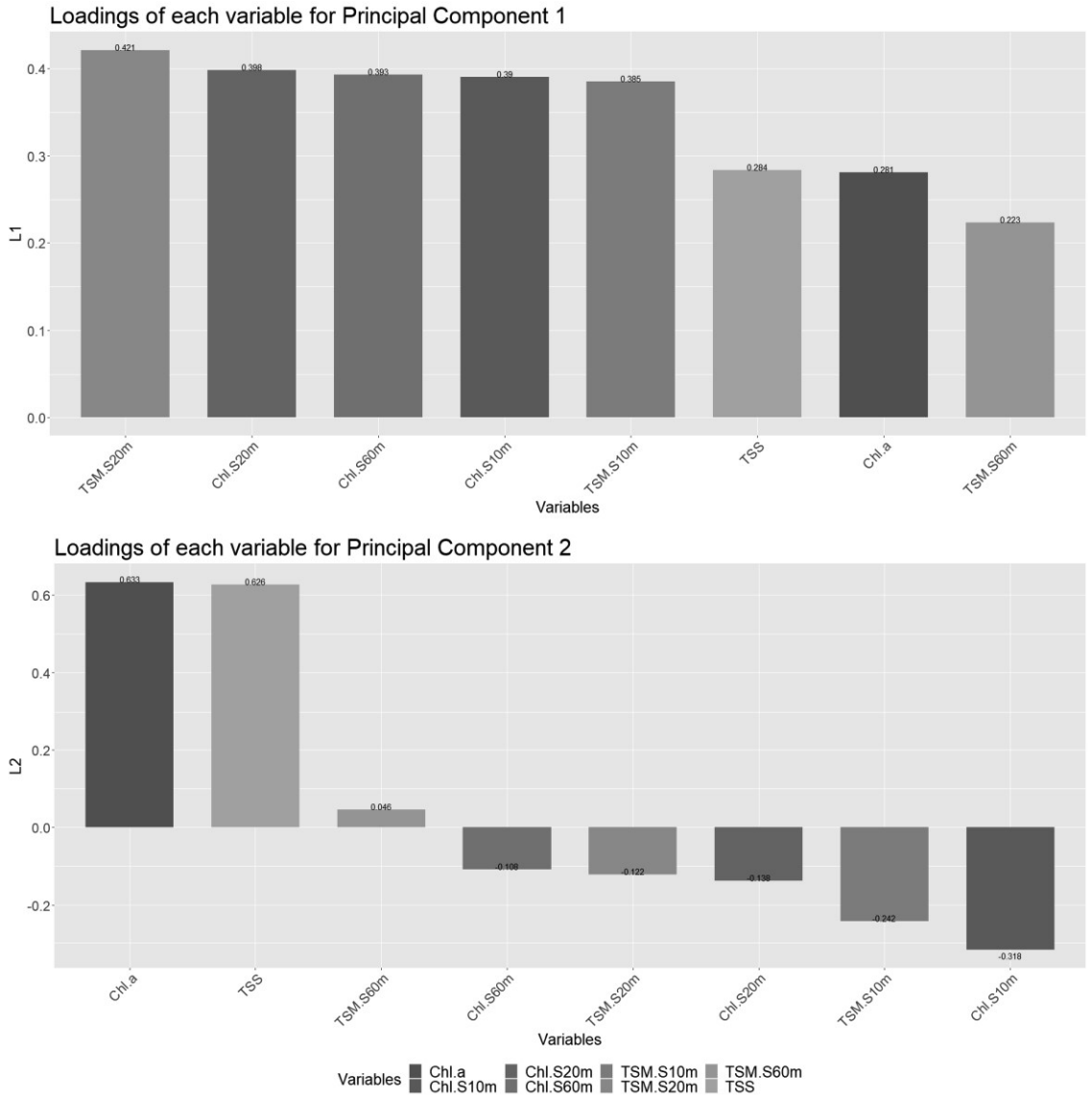

Fig. 31 - Loading scores of both reservoirs [Chl *a*] and [TSS/TSM] *in situ* and satellite variables for PC1 (above) and PC2 (below).

12.Appendix VI - PC scores

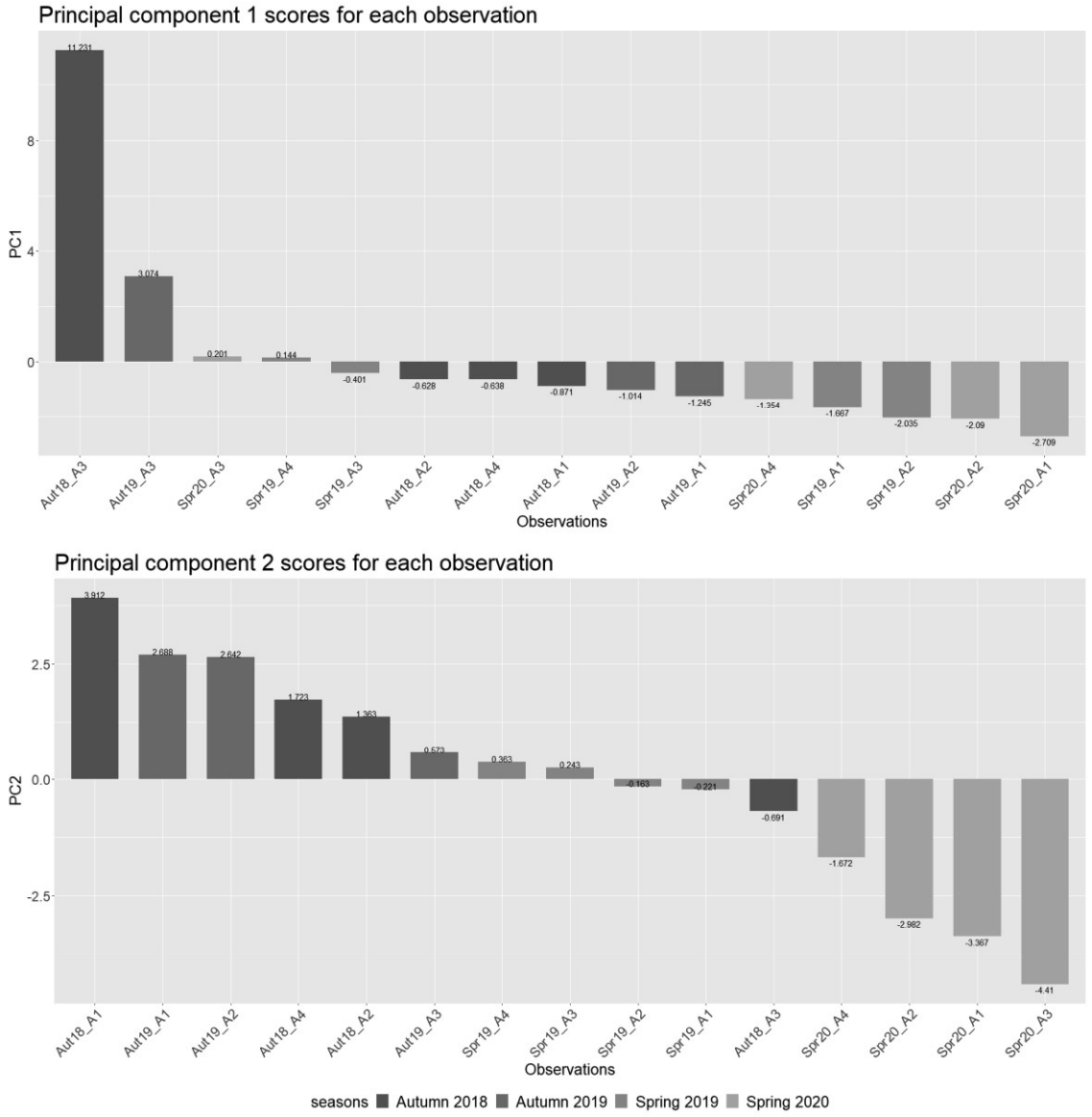

Fig. 32 – From Aguieira's PCA; PC scores of Aguieira observations for PC1 (above) and PC2 (below).

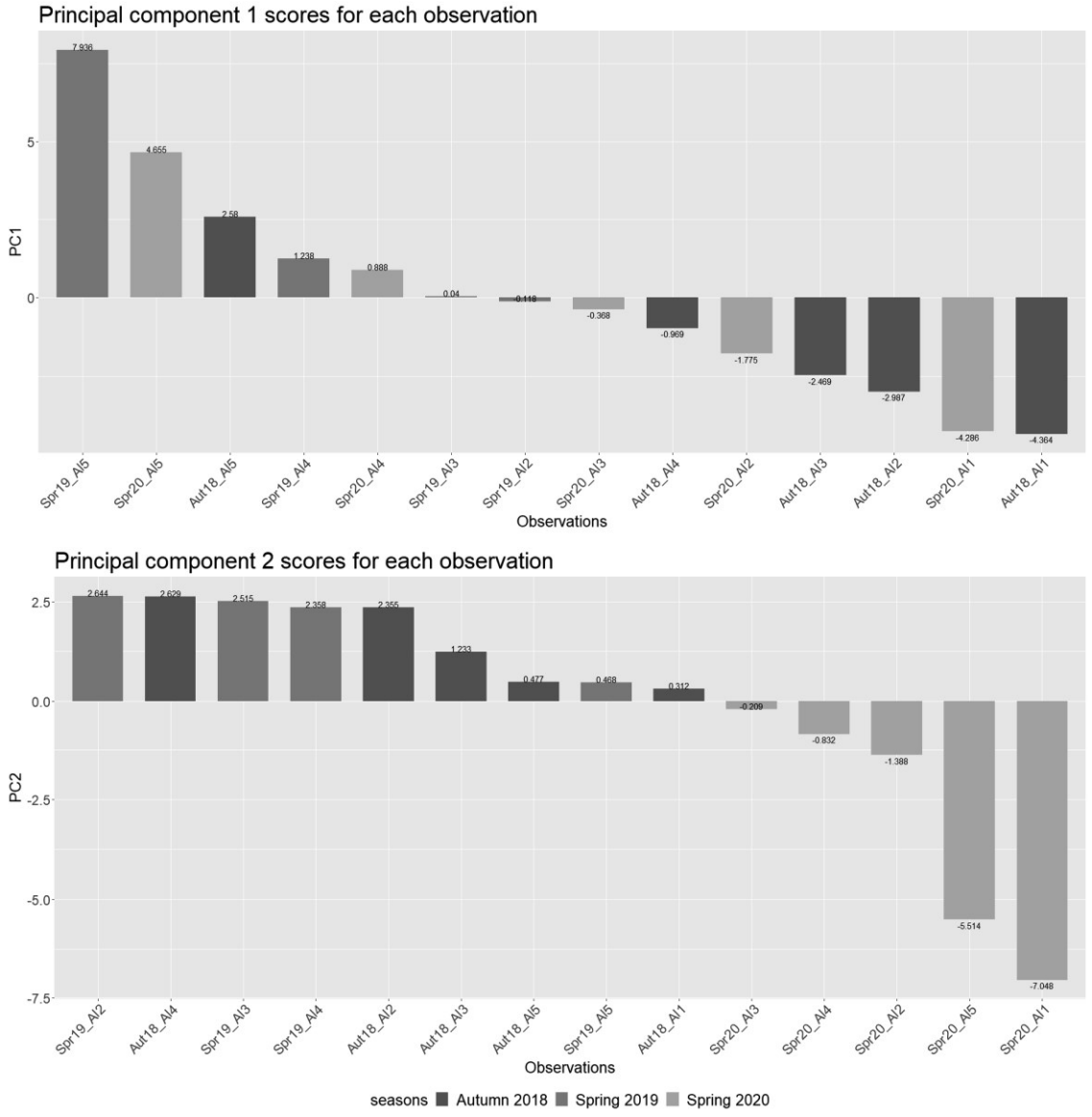

Fig. 33 – From Alqueva's PCA; PC scores of Alqueva observations for PC1 (above) and PC2 (below).

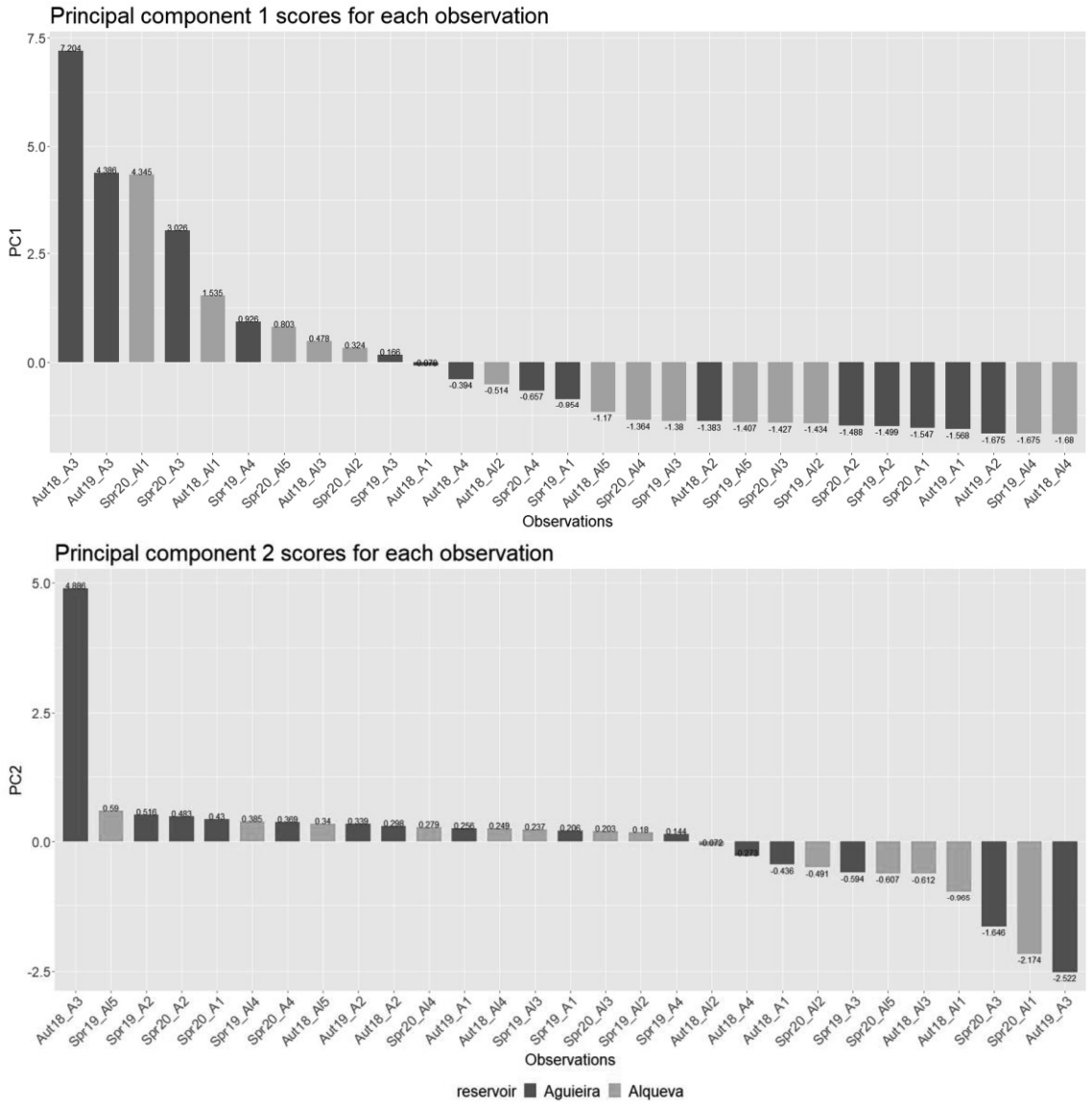

Fig. 34 – From both reservoirs' PCA; PC scores of Aguieira and Alqueva observations for PC1 (above) and PC2 (below).